Rare Earth and Actinide Oxides

Thermodynamic and Electron Miscroscopy Studies

Sørensen, Ole Toft

Publication date:
1975

Document Version
Publisher's PDF, also known as Version of record

Risø Report No. 331

Risø Report No. 331

Danish Atomic Energy Commission

Research Establishment Risø

Rare Earth and Actinide Oxides

Thermodynamic and Electron Microscopy Studies

by O. Toft Sørensen

October 1975

Sales distributors: Jul. Gjellerup, 87, Sølvgade, DK-1307 Copenhagen K, Denmark

Available on exchange from: Library, Danish Atomic Energy Commission, Risø, DK-4000 Roskilde, Denmark

INIS Descriptors

[0] FREE ENERGY
ORDER-DISORDER TRANSFORMATIONS
PHASE DIAGRAMS
PHASE STUDIES
THERMAL GRAVIMETRIC ANALYSIS
THERMODYNAMIC PROPERTIES
VACANCIES
VERY HIGH TEMPERATURE

[1,2] CERIUM OXIDES
SUPERLATTICES

[1] HIGH TEMPERATURE
X-RAY DIFFRACTION

[2] ELECTRON MICROSCOPY
MONOCRYSTALS

[3] BINARY MIXTURES
PLUTONIUM DIOXIDE
URANIUM OXIDES

UDC 546.655-31 : 546.791.4-31 : 546.799.4-31 : 536.7

October 1975 Risø Report No. 331

RARE EARTH AND ACTINIDE OXIDES

Thermodynamic and Electron Microscopy Studies

by

O. Toft Sørensen

Metallurgy Department
Danish Atomic Energy Commission
Research Establishment Risø
Roskilde

ISBN 87 550 0360 5

ISBN 87 550 0362 1 (Thesis)

Abstract

Partial molar thermodynamic quantities for oxygen in sub-stoichiometric cerium oxides (CeO_{2-x}), plutonium oxides (PuO_{2-x}) and mixed uranium-plutonium oxides ($(U, Pu)O_{2-x}$) were determined by thermogravimetric analysis in atmospheres of controlled oxygen pressures (CO_2/CO mixtures) in the temperature range 900-1450°C. Detailed analysis of the data obtained showed that the non-stoichiometric phase ranges for the three oxide-systems, which were previously described as a single, grossly non-stoichiometric phase, can be divided into several subregions each consisting of an apparent non-stoichiometric single phase. The finer details of the thermodynamic data, however, suggest that some of these subregions can be further split into ordered intermediate phases with compositions following the series $M_n O_{2n-2}$.

In order to verify some of the thermodynamic findings, supplementary high-temperature X-ray diffraction studies were made on CeO_2 at temperatures up to 855°C. At the higher temperatures between 790 and 855°C, a new phase of low symmetry was obtained. Indexing the powder pattern for this phase showed it to be isostructural with Pr_6O_{11} and with a monoclinic unit cell with $a = 6.781 \pm 0.006$ Å, $b = 11.893 \pm 0.009$ Å, $c = 15.823 \pm 0.015$ Å and $\beta = 125.04 \pm 0.04°$. The Ce_6O_{11} phase observed in the X-ray studies corresponds to one of the intermediate phases inferred from the thermodynamic data.

Supplementary high resolution electron microscopy studies were also conducted on reduced single crystals of CeO_2. On some particles reduced by beam heating in the microscope, a lamellae structure was observed and a model involving crystallographic shearing is proposed to explain this observation. In other beam-heated particles diffraction patterns were observed corresponding to the monoclinic superstructure found in the high-temperature X-ray studies. Finally patterns on particles reduced by a heat treatment in vacuum under well defined conditions showed that twinning can also take place in this oxide system.

CONTENTS

PREFACE

Rare earth oxides as well as actinide oxides can exist as non-stoichiometric compounds with large deviations from stoichiometry. Today it is well established that the properties of these oxides depend on the nature and number of defects present at the non-stoichiometric composition, and in order to understand the behaviour of these oxides it is necessary to have a detailed knowledge of their defect structure.

In the present work, which was conducted on non-stoichiometric cerium dioxides (CeO_{2-x}), plutonium dioxides (PuO_{2-x}) and on mixed uranium-plutonium dioxides ($(U_{1-y}, Pu_y)O_{2-x}$), these oxides were studied by thermogravimetric analysis in atmospheres of controlled oxygen pressures, by high temperature X-ray diffraction analysis, and by electron microscopy and the results obtained, which have been partly published in five papers, are reviewed in some detail in this thesis. The five papers, also given in the reference list as 1-5, are the following:

1. O. Toft Sørensen, Thermogravimetric Studies of the High Temperature Thermodynamic Properties of Nonstoichiometric Cerium Oxides. In: Proceedings of the 3rd International Conference on Thermal Analysis, held in Davos, 1971. Edited by H. G. Wiedemann (Birkhäuser, Basel, 1972) 31-42.

2. O. Toft Sørensen, Thermodynamic Studies of the Phase Relationships of Non-Stoichiometric Cerium Oxides at Higher Temperatures. To be published in J. Solid State Chemistry.

3. O. Toft Sørensen, High Temperature Studies of Thermodynamic Properties and Structures of Non-Stoichiometric Cerium Oxides, Paper presented at the "4th Nordic High Temperature Symposium" June 1975 in Helsinki, Finland. To be published.

4. O. Toft Sørensen, Studies of Non-Stoichiometric Oxides by Thermoanalytical Methods, Paper presented at Thermoanalytical Symposium in Kassel in June 1975. To be published in Thermochimica Acta.

5. O. Toft Sørensen, Thermodynamic Studies at Higher Temperatures of the Phase Relationships of Substoichiometric Plutonium and Uranium/Plutonium Oxides, Paper presented at the 5th International Conference on Plutonium and Other Actinides, September 1975 in Baden-Baden, Germany. To be published.

The studies are reviewed in three parts. In the first two parts a review is given of the thermogravimetric analysis and high temperature X-ray measurements on cerium dioxides and on plutonium oxides respectively; a literature survey of previous work on these oxide systems is also given as background information. The third part describes in greater detail the electron microscopy examination, which was carried out on CeO_2 single crystals, since this part of the investigation has not yet been published.

Within the framework of Swedish/Danish collaboration on plutonium I spent some $2\frac{1}{2}$ years at the Swedish Atomic Energy Research Centre, Studsvik. During this period, which I found very inspiring, I came into close contact with Swedish atomic energy research, and because a substantial part of the experimental work described in this thesis was carried out at Studsvik, it is natural for me to present this thesis in Sweden. At Studsvik I collaborated and still enjoy collaboration with section MB (Fuel Material Section), and I should like to acknowledge the great help I have received from the staff of this section. In particular I wish to thank G. Berggren for his support and interest in my work. While in Sweden I also came into close contact with the oxide research headed by Dr. Sten Andersson at the University of Lund. This research is well known for its outstanding quality, and contact with this group proved a great inspiration for my own work, and I wish to thank Dr. Andersson for the stimulating discussions we have had both during the experimental work and during the preparation of this thesis.

Extensive thermogravimetric experiments were also carried out in the Metallurgy Department at Risø and here the help of H. Jensen is gratefully acknowledged. I also wish to thank J. Lindbo and J. B. Bilde-Sørensen for their valuable assistance during the electron microscopy examination. Furthermore, I am deeply indebted to Dr. N. Hansen, Head of the Metallurgy Department at Risø, first of all for his continued support and interest in these studies, and secondly for the excellent collaboration we have had on many projects.

Many thanks are also due to Mrs. J. Starcke for revising the English of many of my publications and of this thesis, and to Mrs. K. Hansen and Mrs. I Frydendahl for typing the manuscripts. Finally I am grateful to Mrs. T. Skov and Mr. V. Vegenfeldt of the Drawing Office, who drew many of the plots and diagrams shown in this thesis.

1. INTRODUCTION

In classical chemistry and crystallography it was assumed that inorganic compounds had definite compositions determined by the valence of the atoms and that the atoms were arranged in an ideal structure with all sites occupied. From the early 1900's many inorganic compounds were, however, found to be of variable composition and today it is recognized that an exact stoichiometric composition can only be obtained at definite partial pressures of the components at a given temperature. Deviations from stoichiometric composition are also very common in the inorganic oxides; especially for the oxide systems where the cations can exist in several valence states, such as the oxides considered in this thesis, large deviations have been observed at higher temperatures.

Previously, deviations from stoichiometric composition were explained in terms of defects that, according to the classical defect theories, were considered to be randomly distributed and non-interacting. Different types of defect can be envisaged formed in these non-stoichiometric oxides that, according to Kofstad (6), can generally be classified into:

(1) Oxygen-deficient oxides, e.g. CeO_{2-x}, PuO_{2-x}, in which oxygen vacancies ($V_O^{\cdot\cdot}$) are predominantly formed. The excess of metal has also been considered to arise from the presence of interstitial metal ions ($M_i^{\cdot\cdot\cdot\cdot}$), but experimental evidence strongly in favour of the vacancy model has been obtained for many systems.

(2) Metal-deficient oxides, e.g. $Fe_{1-y}O$, $Mn_{1-y}O$, in which metal vacancies (V_M'') or interstitial oxygen ions (O_i''), as in UO_{2+x}, are predominantly formed.

According to these theories the non-stoichiometric phase regions were described as grossly non-stoichiometric single phase regions, even when they extend over a considerable composition range. For the large concentrations of defects to be expected at substantial deviations from stoichiometry, however, it is inconceivable that these assumptions are fulfilled. On the contrary, clustering, long-range ordering into superstructures or perhaps even elimination of the defects by a crystallographic shearing mechanism, as proposed by Bursill and Hyde for the TiO_{2-x} system (7), should be expected. In accordance with these ideas, recent thermogravimetric analyses of the non-stoichiometry in other oxide systems - PrO_{2-x} (8) for instance - have shown that the non-stoichiometric phase regions for these oxides can be divided into several subregions, and the assumptions

made in classical defect theories are obviously incorrect. For CeO_{2-x}, PuO_{2-x} and $(U_{1-y}Pu_y)O_{2-x}$ the non-stoichiometric phases were also previously considered as single, grossly non-stoichiometric phases and the main purpose of this work is to provide more data for these oxide systems in order to examine the nature of their non-stoichiometric phases at higher temperatures (900-1400°C).

In research on fuel materials for nuclear power reactors - UO_2, PuO_2 and (U, Pu)O_2 - CeO_2 is often used as a model substance for PuO_2, which is an extremely poisonous material to work with. This is justified to a certain extent since these oxides have comparable thermodynamic properties and the same structures, as pointed out by Blank (9). It is, however, a question whether this comparison is still valid if the finer details of the two oxides are considered, and the second purpose of the present investigation was thus to evaluate to what extent the non-stoichiometric phases of the two oxide systems do really have comparable properties.

Finally, as PrO_{2-x}, CeO_{2-x} is an interesting model substance for non-stoichiometric oxides with structures derived from the fluorite structure. Many thermodynamic studies have already been performed both on the PrO_{2-x} system (Hyde et al. (10)) and on CeO_{2-x}, but a thorough investigation of the structures of these non-stoichiometric oxides, for instance by electron microscopy, is still lacking. It must be realized that the thermogravimetric technique used in the study of the thermodynamic properties of these oxides is only an indirect technique, and the conclusions concerning phase relationships and structures drawn from these investigations need to be verified by more direct methods. A further purpose of the present work was therefore to provide some information on the structural relationships in these oxide systems in order to verify some of the conclusions drawn from the thermodynamic experiments. However, it must be admitted that these investigations can only be considered preliminary, and that they only show some aspects of the system. In particular, thorough electron microscopy examinations of these fluorite-related oxides appear to be a very fertile field for future research.

2. THERMODYNAMIC STUDIES OF THE PHASE RELATIONSHIPS OF NON-STOICHIOMETRIC CERIUM OXIDES AT HIGHER TEMPERATURES

Detailed thermogravimetric and structural studies of the Ce-O (11), Pr-O (10) and Tb-O (12) systems have shown that ordered "stoichiometric" phases of the series M_nO_{2n-2} are formed at lower temperatures for these rare earth oxides. At higher temperatures these ordered phases are transformed into non-stoichiometric phases each having a wide composition range as shown in fig.1, which gives the accepted phase diagram of the $CeO_{2.00}$-Ce_2O_3-system proposed by Bevan and Kordis (11).

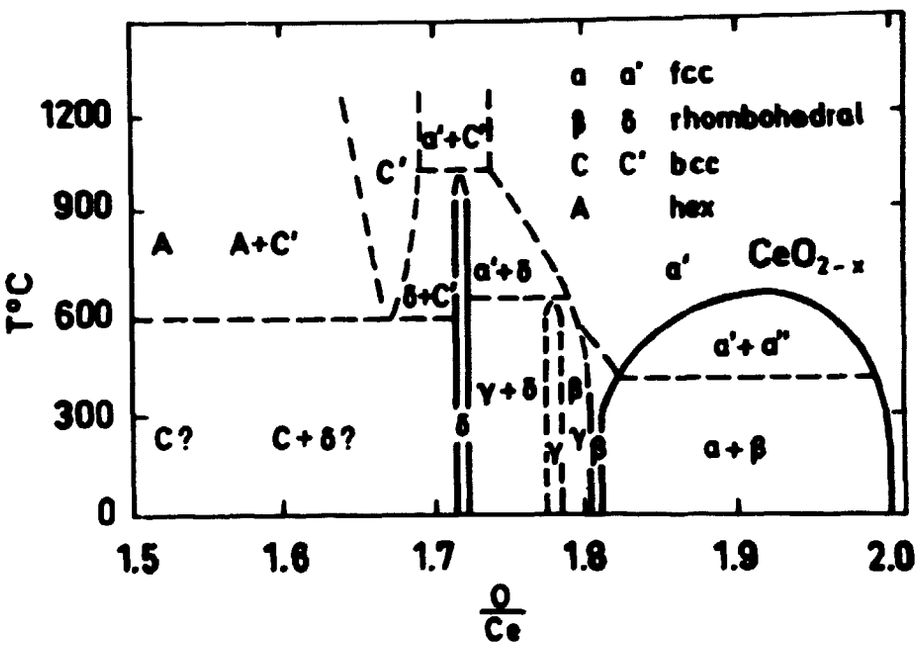

Fig. 1. Phase diagram for the cerium-oxygen system.

As described in (1 - 4), the thermodynamic data for the non-stoichiometric α'-phase were in the present work determined by thermogravimetric analysis in atmospheres of controlled oxygen pressures (CO_2/CO mixtures). The temperature range covered was 900-1400°C and compositions between $CeO_{2.00}$ and $CeO_{1.75}$ could be reached with the gas mixtures used. Furthermore, in order to obtain information about the structures of non-stoichiometric phases of this system, a few high temperature X-ray diffraction measurements were carried out. Unfortunately it was not possible to work with gas mixtures of controlled oxygen pressures in the high temperature X-ray equipment available, and these measurements were therefore per-

formed in vacuum.

2.1. Previous Studies

2.1.1. Phase Relationships

Various methods were previously used in thermodynamic studies of cerium oxides in order to determine the phase relationships of these oxides. Kuznetsov et al. (13), for instance, used the emf technique, whereas Brauer et al. (14) used a technique by which the composition was determined by intermittent weighing at room temperature after the samples were equilibrated in various H_2/H_2O mixtures at temperatures between 600-1000°C. A better method is the thermogravimetric analysis used by Bevan and Kordis (11) in their detailed study of the cerium oxides by equilibration experiments both in CO/CO_2- and in H_2/H_2O-mixtures in the temperature range 636-1169°C. Based on the thermodynamic data obtained and on previous data, Bevan and Kordis constructed the phase diagram shown in fig. 1, which has remained the accepted diagram for the CeO_2-Ce_2O_3 system. Using X-ray powder pattern techniques, Bevan (15) was the first to provide detailed evidence of a sequence of intermediate rhombohedral phases in this system. In this study the samples were reduced in flowing hydrogen and then annealed in vacuum at 1050°C before they were quenched for X-ray diffraction analysis at room temperature. Finally, in a later study Brauer and Gingerich (16) showed by high temperature X-ray diffractometry that the miscibility gap below the α'-region shown in the diagram closes at 685°C at a composition of $CeO_{1.92}$.

Recently further thermodynamic studies on cerium oxides have been carried out in the temperature range 900-1300°C by Iwasaki and Katsura (17) using the thermogravimetric equilibration technique and covering the composition range $CeO_{2.00}$-$CeO_{1.70}$. Here the α'-phase was considered as a solid solution of CeO_2 and Ce_2O_3. The activities of these two components in the solution were calculated from the thermogravimetric data as a function of composition at the different temperatures used. For small Ce_2O_3 concentrations at temperatures above 1200°C, it was found that the activity of CeO_2 followed Raoult's law, whereas the activity of Ce_2O_3 followed Henry's law in this range. This ideal behaviour was not observed at higher concentration of Ce_2O_3 and at lower temperatures, however, and it is probably too simple to treat the α'-phase in this way.

Usually the relative partial enthalpies of oxygen ($\Delta\overline{H}_{O_2}$) are calculated from the measured relative partial free energies of oxygen ($\Delta\overline{G}_{O_2}$), but in a recent study Campserveux and Gerdanian (18) were able to measure

$\Delta\overline{H}_{O_2}$ directly by microcalorimetry. In their study, which was carried out at 1353 K (1080°C), the whole composition range CeO_2 to Ce_2O_3 was covered. Results were obtained in good agreement with those reported by Bevan and Kordis (11).

2.1.2.Defect Models

The non-stoichiometric cerium oxides, CeO_{2-x}, are oxygen-deficient oxides in which, in previous studies, the non-stoichiometry was considered to be due to either interstitial cerium ions or ionized oxygen vacancies. In these studies the compositions of the oxides are plotted as a function of their equilibrium oxygen pressures, and an oxygen pressure dependence of $x \propto p_{O_2}^{-1/n}$ is observed where the value of n depends on the type of predominant defect present in the oxide. In a study of the electrical conductivity of CeO_{2-x} as a function of oxygen pressure in the temperature range 650-1400°C, Greener et al. (19) found a pressure dependence of $p_{O_2}^{-1/5}$. To explain this the authors suggested that the predominating defects are either quadruply ionized cerium interstitials or completely ionized oxygen vacancy pairs. Considering the data of Greener et al. together with those reported by Bevan and Kordis (11), Kevane (20), however, concluded that the results are best described by a model involving single-charged oxygen vacancies near the stoichiometric composition (high oxygen pressures) and neutral vacancies in more reduced oxides. In a similar but more extensive study of the electrical conductivity of CeO_{2-x} in the temperature range 800-1500°C, Blumenthal and Laubach (21) also found a pressure dependence consistent with a vacancy model involving multiple states of ionization. However, in a later study extended to lower oxygen pressures (10^{-21} atm), Blumenthal et al. (22) interpreted their conductivity data in terms of triply and quadruply ionized cerium interstitials. Other models have also been proposed to explain the non-stoichiometric behaviour of the cerium oxides. For instance, Kofstad and Hed (23) found that the data of Bevan and Kordis could be interpreted by a model involving singly and doubly ionized cerium interstitials and electrons localized on cerium ions on normal lattice sites. By assuming that the electrons have only a small probability of occupying nearest neighbours to the interstitial cerium ions, Kofstad and Hed introduced a site blocking effect to explain the increase in n observed at larger deviations from stoichiometry.

From none of these previous studies was it possible to conclude firmly whether the predominant defects are interstitial cerium ions or oxygen vacancies; although the results obtained recently by Steele and Floyd (24)

in measurements of the oxygen self-diffusion in CeO_{2-x} from 850-1150°C finally seem to support an oxygen vacancy model for these oxides. Unfortunately the measurements of Steele and Floyd were not sensitive enough to detect the degree of ionization of the vacancies, but from a thermodynamic study of CeO_{2-x} Panlener and Blumenthal (25) concluded that doubly ionized oxygen vacancies predominate near the stoichiometric composition.

The major limitation of the studies described so far is that they assume a random distribution of the defects and neglect the long-range defect-defect interactions, which can be expected to become important at larger deviations from stoichiometry. In order to take these effects into account, Atlas (26) proposed a statistical model in which partial ordering of singly ionized oxygen vacancies and localized electrons is considered. The $\Delta\overline{G}_{O_2}$ values calculated from this model were compared to the data reported by Bevan and Kordis and, although they were shown to reflect the major experimental trends, quite large differences in the calculated and observed thermodynamic quantities were observed indicating that even this model is too crude to describe the complex behaviour of these oxides.

2.2. Thermogravimetric Analysis: Experimental

2.2.1. Starting Material

The cerium oxide used as starting material was Fluka CeO_2, reagent grade. As described in (1), spectroscopic X-ray fluorescence analysis showed this material to be very pure. By X-ray diffraction analysis a lattice parameter of $a_o = 5.4115 \pm 0.0003$ Å was determined for this material, corresponding to the value reported by Bevan and Kordis (11) for stoichiometric, purified CeO_2.

2.2.2. Experimental Conditions

The experimental set-up used in the thermogravimetric analysis, which has been described in (1), is shown in fig. 2.

The equipment consists of:

(a) A Netzsch thermobalance with an accuracy of $\pm$ 0.2 mg and with a temperature range of 20-1550°C. An Al_2O_3 crucible was used as sample holder.

(b) A gas system for purification and mixing of CO_2 and CO in the ratio corresponding to the desired oxygen pressure. CO_2/CO ratios between 1/1000 and 1000/1 could be obtained in this equipment. The CO_2/CO ratio was checked occasionally by gas chromatographic measurements.

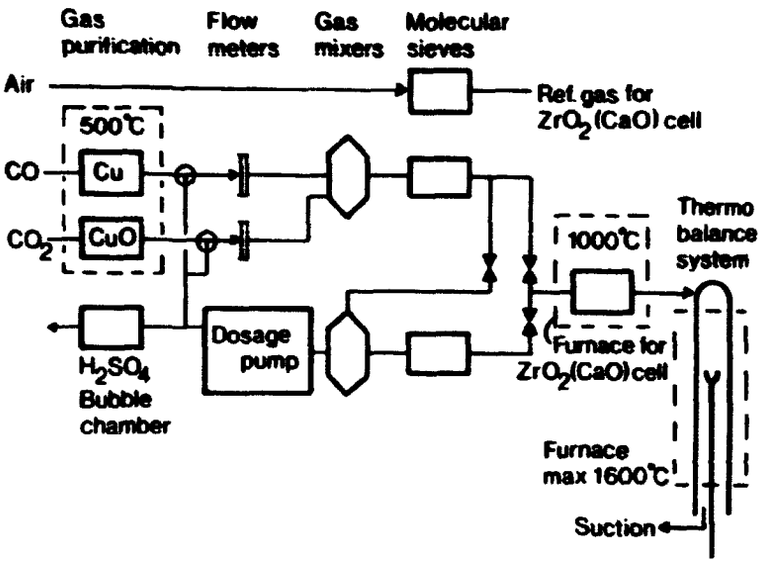

Fig. 2. Experimental set-up for thermogravimetric analysis of CeO_{2-x} in controlled atmospheres.

(c) A ZrO_2(CaO) solid electrolyte cell for a continuous control of the oxygen pressure of the atmospheres used. This cell was placed in a separate furnace operated at 1000°C. The principle and calibration of the cell are described in the appendix.

Before each run with cerium oxide, the corrections due to changes in the buoyancy with temperature were determined with an empty crucible for each atmosphere used. After correction, the experimental error in the oxide composition - x in CeO_{2-x} - can be judged to be $\pm$ 0.003. For the oxygen pressures determined by the ZrO_2(CaO) cell, the accuracy is judged to be $\Delta(\log p_{O_2}) = \pm 0.035$, corresponding to an error in $\Delta\overline{G}_{O_2}$ of $\pm$ 200 cal/mole at 1000°C.

Several types of experiment were performed:

(a) Isothermal experiments in which the samples were treated in different atmospheres at fixed temperatures until equilibrium was obtained. The atmospheres used in these experiments were CO_2/CO: 1000/1 - 1/1000.

(b) Continuous heating and cooling of the sample in atmospheres of fixed composition - CO_2/CO: 6/1, 4/1, 2.5/1, 1/1, 1/2.8, 1/4.5, 1/6, 1/10.

(c) Continuous heating and cooling of the sample in atmospheres of fixed oxygen pressure. This was obtained by changing the CO_2/CO ratio at short intervals in a precalculated manner in order to keep the oxygen pressure constant as the temperature changed. This type of exper-

iment is particularly useful to establish the existence of two-phase regions and of discrete ordered phases as pointed out by Hyde (10). Atmospheres used: CO_2/CO: 30/1-1/110.

In the experiments a slow heating rate of 1°/min was used in order to maintain equilibrium between the sample and the atmosphere during the run. It is of course questionable whether the chosen heating rate is low enough to assure this equilibrium, but according to previous experience (11) it is generally accepted that the cerium oxides respond rapidly to changes in oxygen pressures even at relatively low temperatures. In order to check this point several runs were carried out with the same atmosphere but with heating rates between 1 and 10°/min. These experiments showed that there was no change in the compositions reached at given temperatures at and below a heating rate of 2°C/min, and the chosen heating rate of 1°C/min is believed to be sufficiently low to maintain equilibrium.

2.2.3. Calculations of Sample Compositions

After the sample weights plotted during the thermogravimetric experiments were corrected for buoyancy effects, the compositions of the samples were calculated from:

$$O/M = 2-x = \frac{W_S \cdot M_{CeO_2}}{W_{CeO_2} \cdot 16} - \frac{M_{Ce}}{16} = W_S \cdot k_1 - k_2 \qquad (1)$$

where W_S represents the weight of the sample, W_{CeO_2} the weight of the sample in the stoichiometric reference state, M_{CeO_2} and M_{Ce} the molecular weights of CeO_2 and Ce, respectively, and k_1 and k_2 constants that can be calculated after determining W_{CeO_2}.

2.2.4. Calculation of Thermodynamic Data

Using the oxygen pressures determined for the atmospheres in equilibrium with the samples, the important thermodynamic quantity, $\Delta\overline{G}_{O_2}$ (relative partial free energy of oxygen), was calculated by the relation:

$$\Delta\overline{G}_{O_2} = RT \ln p_{O_2}, \qquad (2)$$

whereas the relative partial entropies, $\Delta\overline{S}_{O_2}$, and the relative partial enthalpies, $\Delta\overline{H}_{O_2}$, were calculated from the standard thermodynamic equations:

$$\Delta\bar{S}_{O_2} = - \frac{\partial(\Delta\bar{G}_{O_2})}{\partial T} \qquad (3)$$

$$\Delta\bar{H}_{O_2} = \Delta\bar{G}_{O_2} + T\Delta\bar{S}_{O_2} \, . \qquad (4)$$

According to the defect theories (6), the formation of oxygen vacancies can be expressed by the reaction

$$O_O + 2M_M = V_O^{\cdot\cdot} + 2M'_M + 1/2\ O_2 \qquad (5)$$

where, according to Kröger's notation (27), O_O and M_M represent oxygen and metal atoms on their respective sites in the crystal lattice, $V_O^{\cdot\cdot}$ represents a double positively charged oxygen vacancy and M'_M a negatively charged metal ion (e.g. Ce^{3+} which is negative relative to the normal lattice with Ce^{4+}) in the normal cation lattice, which has taken up one of the electrons liberated during ionization of the oxygen vacancies. By assuming that the law of mass action is valid for this equilibrium, by introducing the neutrality condition

$$[M'_M] = 2[V_O^{\cdot\cdot}] \qquad (6)$$

and finally by expressing $[V_O^{\cdot\cdot}]$ as the fraction of unoccupied sites in the oxygen lattice, i.e. $[V_O^{\cdot\cdot}] = \frac{x}{2}$, it can be shown that the composition of the oxides should depend on the oxygen pressure according to $x \propto p_{O_2}^{-1/6}$. If the oxygen vacancies are only singly charged the exponent of this proportionality will be -1/4, whereas neutral vacancies will give -1/2. Other exponents can be derived for other types of defects or defect clusters, but generally $x \propto p_{O_2}^{-1/n}$, which substituted into eq. (2) gives:

$$\Delta\bar{G}_{O_2} \propto -n\,RT\,\ln x. \qquad (7)$$

If this treatment is valid a linear relationship should be found when $\Delta\bar{G}_{O_2}$ is plotted against ln x at constant temperature if n is constant, i.e. if one type of defect prevails in a subregion within the non-stoichiometric phase range. From the experimental errors on x and $\Delta\bar{G}_{O_2}$ given in section 2.2.2, the error in n calculated from this equation can be judged to be $\pm$ 0.25.

2.2.5. Free Energy of Formation of CeO_{2-x}

In a study of the phase relationships of a system it is often helpful to consider the free energies of formation of the phases, as the most stable phases will be those with the lowest free energy. Data for the free energy of formation of CeO_2 and Ce_2O_3 have been summarized by Holley et al. (28) for the temperature range 100-1400 K, but data for CeO_{2-x} as a function of composition and temperature are still lacking.

According to Balesdent (29), the standard free energy for the reaction

$$CeO_{2-x} + \frac{x}{2} O_2 = CeO_2 \qquad (8)$$

can be calculated from

$$\Delta G^o = \frac{RT}{2} \int_{2-x}^{2.00} \ln p_{O_2} \, d(2-x) . \qquad (9)$$

It can also be expressed by the standard free energy of formation of CeO_2 and CeO_{2-x} respectively by

$$\Delta G^o = \Delta G_f^o(CeO_2) - \Delta G_f^o(CeO_{2-x}) , \qquad (10)$$

which can be rearranged to give

$$\Delta G_f^o(CeO_{2-x}) = \Delta G_f^o(CeO_2) - \Delta G^o , \qquad (11)$$

or if $\Delta \overline{G}_{O_2} = RT \ln p_{O_2}$ is substituted into eq. (11)

$$\Delta G_f^o(CeO_{2-x}) = \Delta G_f^o(CeO_2) - \frac{1}{2} \int_{2-x}^{2.00} \Delta \overline{G}_{O_2} \, d(2-x) . \qquad (12)$$

The free energy of formation of the non-stoichiometric oxides can thus be evaluated by a graphical integration of the $\Delta \overline{G}_{O_2}$ versus (2-x) curve and from published data for $CeO_{2.00}$. In the present work $\Delta G_f^o(CeO_{2-x})$ was only calculated at 1000°C, at which temperature $\Delta G_f^o(CeO_2) = 195,100$ cal/mole according to Holley et al. (28).

2.3. Thermogravimetric Analysis: Results and Discussion

2.3.1. Relative Partial Free Energies, $\Delta\overline{G}_{O_2}$

The $\Delta\overline{G}_{O_2}$ values calculated from the measured equilibrium oxygen pressures are plotted in fig. 3 as a function of the corresponding composition of the CeO_{2-x} samples (log x) determined in the temperature range 900-1400°C, both during heating (reduction) and cooling (oxidation) of the samples. As clearly demonstrated by Bursill and Hyde (30) in their studies of the TiO_x system, many data points are necessary in order to observe the finer details of a non-stoichiometric system. The CeO_{2-x} data obtained in this work are therefore plotted in fig. 3 together with data previously reported by Bevan and Kordis (11), Panlener and Blumenthal (25), and Iwasaki and Katsura (17) in order to take into account the existing thermogravimetric data for this system.

Comparing the results obtained in previous investigations with those obtained in this work, it will be noted that good agreement exists except for the data reported by Iwasaki and Katsura at 900 and 1000°C, of which only a few are shown in fig. 3. Recent emf measurements on cerium oxides by Hampson (31) also disagree with Iwasaki and Katsura's results at lower temperatures, and thus these results were omitted in this treatment.

Considering all the data points in fig. 3 some interesting details are revealed. First of all the straight-line relationship predicted from eq. (7) is clearly observed, but apparently the slope of the lines changes with increasing deviation from the stoichiometric composition. From the slopes of the lines, which depend on the temperature, the corresponding value of n in $x \propto p_{O_2}^{-1/n}$ was calculated; it is also given in fig. 3 for each of the straight lines. Considering these values, the α'-phase can apparently be divided into subregions, which can each be described by a characteristic value of n, indicating that a characteristic defect is apparently formed within each subregion. This subdivision into subregions is better demonstrated in fig. 4 where the composition at the breaks in the lines where the slope changes - which can be taken as an indication of the subregion boundaries - is plotted as a function of temperature in a normal phase diagram.

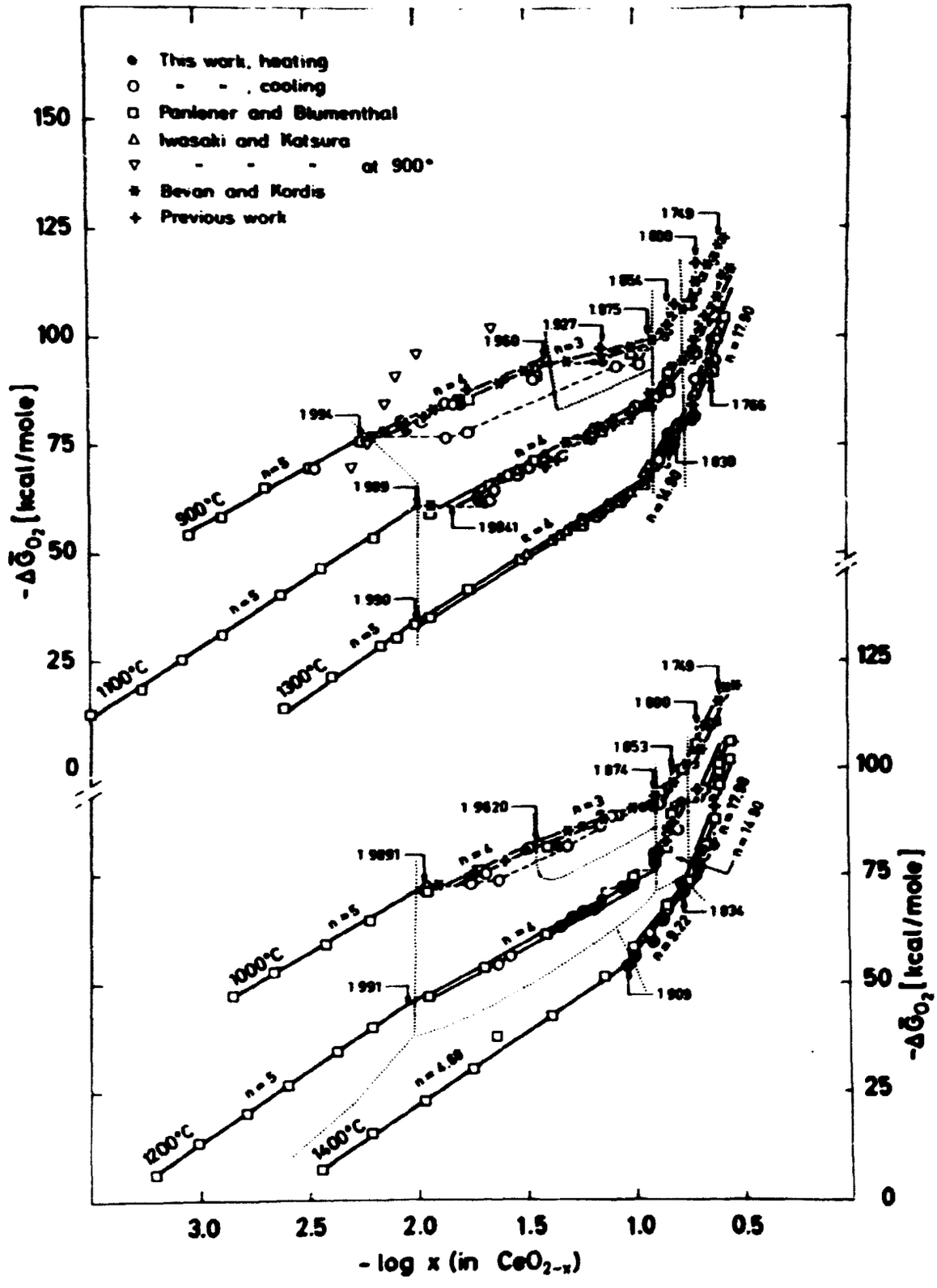

Fig. 3. Relative partial free energies for oxygen, $\Delta\bar{G}_{O_2}$, of CeO_{2-x} as a function of composition (log x).

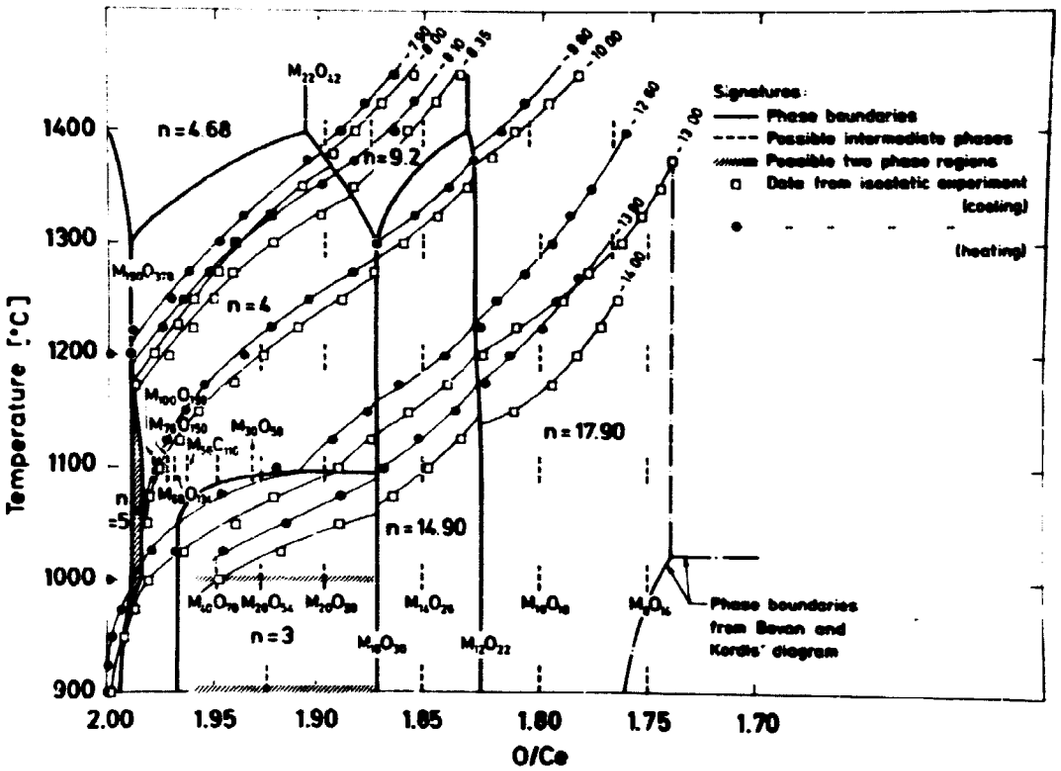

Fig. 4. Diagram of subregions with possible ordered intermediate phases in the α' phase for the Ce-O system.

Recently an improved statistical model for non-stoichiometric fluorite-related oxides was proposed by Manes (32) for PuO_{2-x} and (U, Pu)O_{2-x}. It is interesting to note that the statistical calculations carried out on this model also show that the non-stoichiometric range can be divided into subregions each with a characteristic type of defect. This model assumes that defect complexes consisting of one oxygen vacancy and two metal atoms are formed in the first subregion below the stoichiometric composition. From geometrical considerations of the lattice structure Manes calculated the number of forbidden oxygen positions in which oxygen vacancies cannot be formed surrounding the defect complex, and a limiting concentration of defects can be calculated: O/M = 1.91 was found for the first subregion. By introducing two, three, etc., vacancies in the defect complexes, limiting defect concentrations at O/M = 1.83, 1.74 and 1.65 were obtained. Compared to the compositions of the subregion boundaries found in this work (fig. 4), it will be noted that for both oxide systems a boundary at O/M ~ 1.83 and 1.74 is observed, whereas some disagreement exists regarding the boundary of the first subregion.

In principle it should be possible to interpret the values of n found for the different subregions in terms of types of defect, but this can only be

rather speculative. The region with n = 5, for instance, could be taken as an indication of interstitial metal ions, but today it is generally believed that the cation lattice for these oxides is very stable (33), and this interpretation cannot be correct. By taking enthalpy variations into account - the classical defect theories outlined above assume that the enthalpy of defect formation is constant and independent of composition - it has also been shown (25) that n = 5 could be obtained even with double-charged oxygen vacancies ($V_O^{\cdot\cdot}$) in contrast to the n = 6 value found in the classical defect theories for this defect. However, this again is rather speculative since the defects are considered to be randomly distributed in this approach. Contrary to the single defects, n = 5 has also been interpreted in terms of oxygen vacancy pairs ($V_O^{\cdot\cdot}$, $V_O^{\cdot\cdot}$) from the measurements of electrical conductivity as a function of oxygen pressure for CeO_{2-x} by Greener et al. (19). Although this model is probably also incorrect, it is important because it emphasizes that the interaction between the defects should be taken into account and that defect complexes rather than single defects must be expected in these oxides. The importance of interactions between the defects has also been pointed out in other models. Hyde et al. (34), for instance, proposed for the PrO_{2-x} system that infinite MO_6 strings along the ⟨111⟩ directions are an important structural entity, whereas Thornber et al. (35) proposed that the oxygen vacancies cluster pairwise into units consisting of a central 6-coordinate cation surrounded by six 7-coordinate cations. The central cation in the complex has been reduced to a lower charge (M^{3+}) by the electrons liberated from the oxygen vacancies, and the metal ions thus also seem to play a decisive role, which is important for mixed oxide systems as will be shown for the $(U, Pu)O_2$ system in the next section.

Hysteresis, which plays an important role in other rare earth oxide systems (10), is only observed at 900 and 1000°C for the cerium oxides in the composition range 1.9950-1.8750 (2-x). This suggests that the $\alpha' + \alpha''$ miscibility gap extends to about 1000°C in contrast to 650°C as proposed by Bevan and Kordis (see phase diagram fig. 1). Even at 1000°C this effect is not very pronounced and at higher temperatures a high degree of reversibility was observed in accordance with the observations made by Bevan and Kordis that showed that the cerium oxides are very reactive at higher temperatures.

Considering the phase rule criteria for a binary oxide system in equilibrium with a gas phase, the $\Delta\bar{G}_{O_2}$ versus log x plot can also give information about the phase relationship of the system (36). For a two-phase range, for instance, the system will only have one degree of freedom

and a horizontal line should be observed at constant temperature. Near vertical lines can in the same way be assumed to prove the existence of discrete compounds of a narrow composition range, whereas lines with an intermediate slope indicate the existence of a single non-stoichiometric phase, or a continuous sequence of ordered or partly ordered phases as found for the Ti-O system by Merritt and Hyde (37).

If the $\Delta\overline{G}_{O_2}$ values shown in fig. 3 are considered according to these criteria, the following information can be obtained about the phase relationships in this oxide system:

(1) In some cases a horizontal curve is observed between two subregions instead of a single change in slope indicating that a two-phase region exists between the two regions. Because of the scatter in the data the existence of these two-phase regions is rather uncertain, however, and instead of a horizontal line a gradual change in slope should perhaps be drawn indicating that there is a gradual change in predominant defects at the subregion boundaries.

(2) The subregions can be considered as consisting of apparent non-stoichiometric single phases, whose macroscopic thermodynamic properties can be described by a characteristic value of n. Values of $n \neq 6$ can probably be explained by the formation of common defect types according to the defect theories, but this is not the case for the $n > 6$ values observed below O/M = 1.8750. Analysing the finer details of the data points - the data obtained at 1100°C are shown on a larger scale in fig. 5 - gives a strong indication of the existence of a whole series of discrete phases separated by two-phase regions for these regions. However, even for the $n = 4$ and 3 regions such discrete compounds appear to be possible at lower temperatures. An interesting feature is that most of the compositions of these discrete phases, as well as the main boundaries for the subregions, seem to follow the series M_nO_{2n-2}, which also describes the intermediate phases at lower temperatures (11).

2.3.2. Phase Relationships

The phase relationships of the system can also be studied from a $\Delta\overline{G}_{O_2}$ versus temperature plot at constant composition. In this plot straight lines should be obtained within each subregion whereas a change in the slopes indicates a region boundary. The resulting plot, which is shown in fig. 6, clearly demonstrates this, and from this diagram the boundaries between

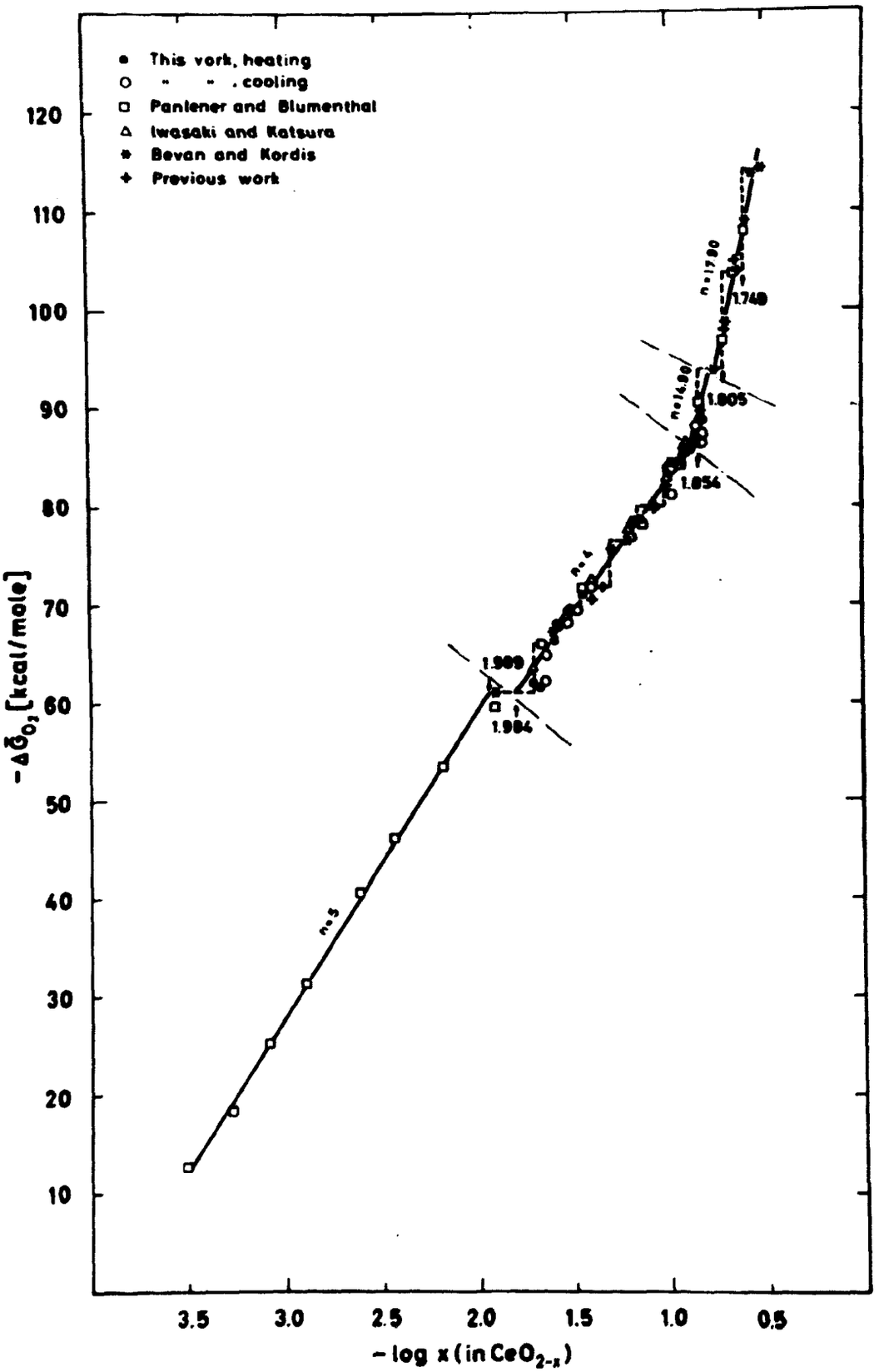

Fig. 5. Relative partial free energies, $\Delta\bar{G}_{O_2}$, at 1100°C of CeO_{2-x} as a function of composition (log x).

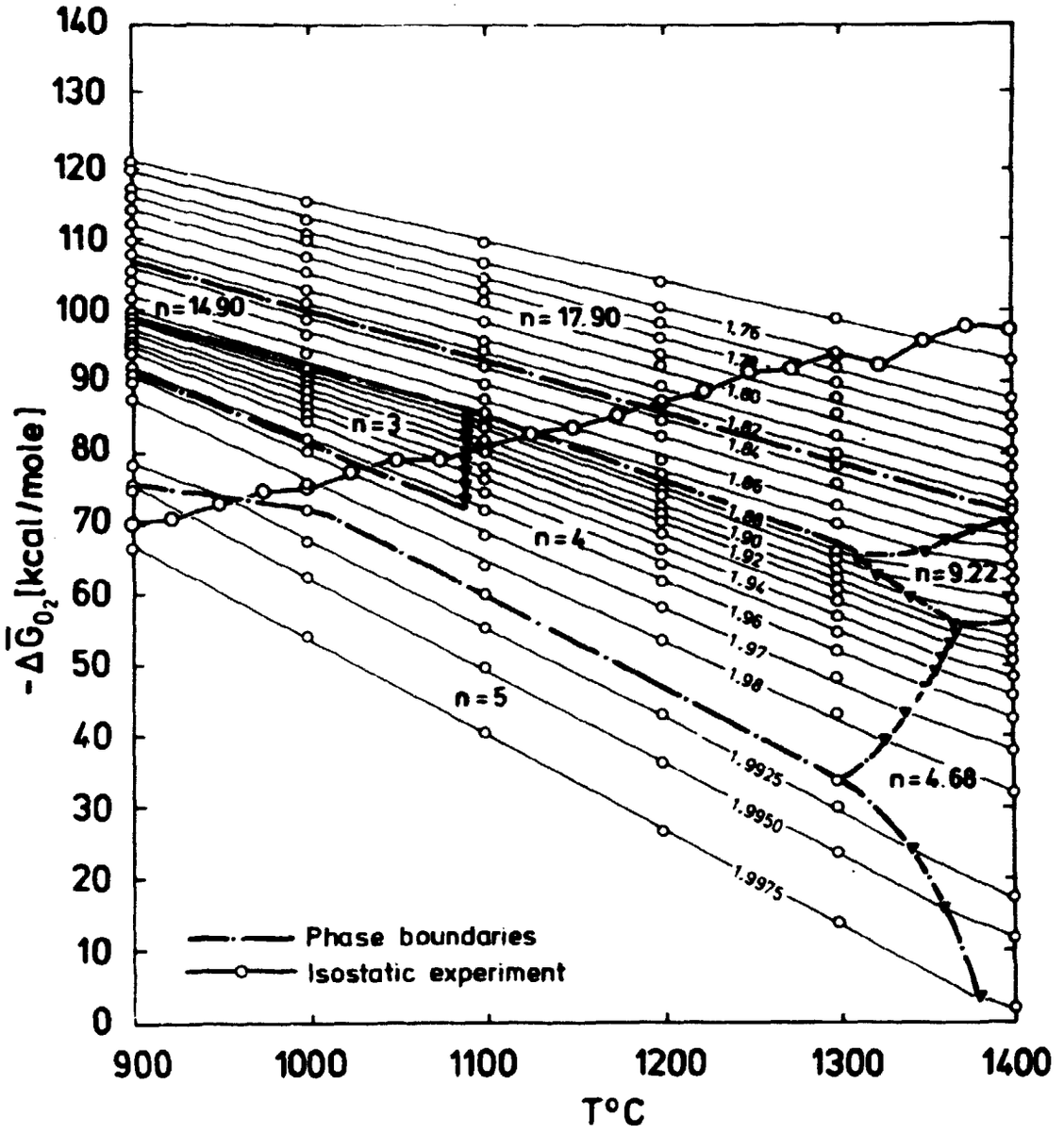

Fig. 6. Relative partial free energies of oxygen, $\Delta\bar{G}_{O_2}$, of CeO_{2-x} as a function of temperature for constant composition.

the different subregions can easily be determined. Previously, straight $\Delta\overline{G}_{O_2}$ versus T lines were always obtained throughout the whole non-stoichiometric α'-phase at higher temperature (11, 25). However, in a recent study by the emf technique, Hampson (31) found that $\Delta\overline{G}_{O_2}$ does not vary linearly with temperature in accordance with the results obtained in this investigation.

The subregion boundaries shown in fig. 6 closely agree with the boundaries shown in the T, x diagram (fig. 4), and the figure again clearly demonstrates that the non-stoichiometric α'-phase should no longer be considered as a grossly non-stoichiometric phase over an extended composition range, but that it can be divided into subregions. The position of the subregion boundaries can also be confirmed by the shape of the diagonal curve obtained in the isostatic experiments. An example of the compositions obtained in these experiments is shown in the $\Delta\overline{G}_{O_2}$ versus T plot in fig. 6. From this it is evident that an exponential variation of x with temperature must be expected for the subregions as the slopes of the $\Delta\overline{G}_{O_2}$-T lines vary within each region. This exponential behaviour of the isobaric data is also clearly seen in the T, x diagram in fig. 4, where a characteristic behaviour is obtained for each of the single subregions and, more important, where the exponential function describing the points seems to change where the subregion boundaries have been observed.

2.3.3. Relative Partial Enthalpies, $\Delta\overline{H}_{O_2}$

The $\Delta\overline{H}_{O_2}$ values calculated according to eq. (4) are shown in fig. 7 as a function of log x. Only for the n = 5 and n = 14, 90 regions is $\Delta\overline{H}_{O_2}$ close to being independent of composition as expected for randomly distributed and independent defects, whereas, for the other phases, $\Delta\overline{H}_{O_2}$ shows linear variations with log x with substantial slopes. Apparently there is a considerable interaction and ordering of the defects in these phases and this must also be taken into account. The calculation was carried out at 1353 K (1080°C) in order to compare the results with the $\Delta\overline{H}_{O_2}$ values reported by Campserveux and Gardenian (18), which were determined by microcalorimetric measurements at this temperature. It it interesting to note that the $\Delta\overline{H}_{O_2}$ values calculated in the present study correspond closely to the experimental values except perhaps for the n = 4 region where the calculated values lie slightly above the experimental ones, but still on a line parallel to the band of experimental data points. The difference, however, is small compared to the experimental errors usually obtained in thermodynamic measurements, and the close correspondence between the

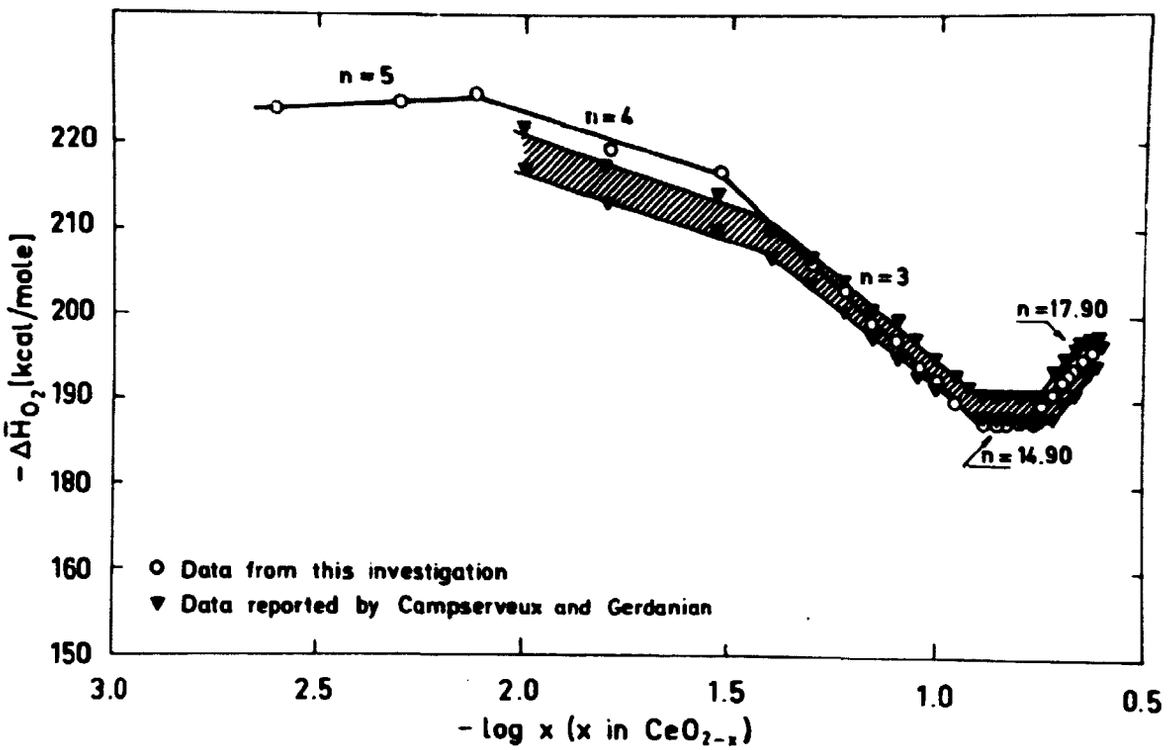

Fig. 7. Relative partial enthalpy of oxygen, $\Delta\bar{H}_{O_2}$, of CeO_{2-x} calculated at 1353 K as a function of composition (log x).

two data sets gives further support to the previous indications of the existence of several subregions in the α'-phase at higher temperatures.

2.3.4. Free Energy of Formation of CeO_{2-x}

The free energy values calculated from eq. (12) are shown in fig. 8 as a function of the mole fraction of oxygen in the oxides calculated from $x_O^* = \frac{(2-x)}{1+(2-x)}$. This plot is particularly useful since the relative partial free energy of oxygen, $\Delta\bar{G}_{O_2}$, for a given composition can be found by extrapolation of the tangent to the curve to $x_O^*=1$, as described by Darken and Gurry (38). For each of the subregions observed at 1000°C (fig. 3), the straight bands were extrapolated outside their composition ranges in order to examine the difference in $\Delta G_f^o(CeO_{2-x})$ where the phases overlap. Although this difference is small, so that essentially a smooth curve is obtained throughout the whole composition range covered as shown in fig. 8, it is evident that the free energies of formation observed for each subregion are lower than those of the neighbouring regions. This indicates that these subregions have greatest stability within their respective range of existence. For the subregion characterized by n = 3, the $\Delta\bar{G}_{O_2}$ versus

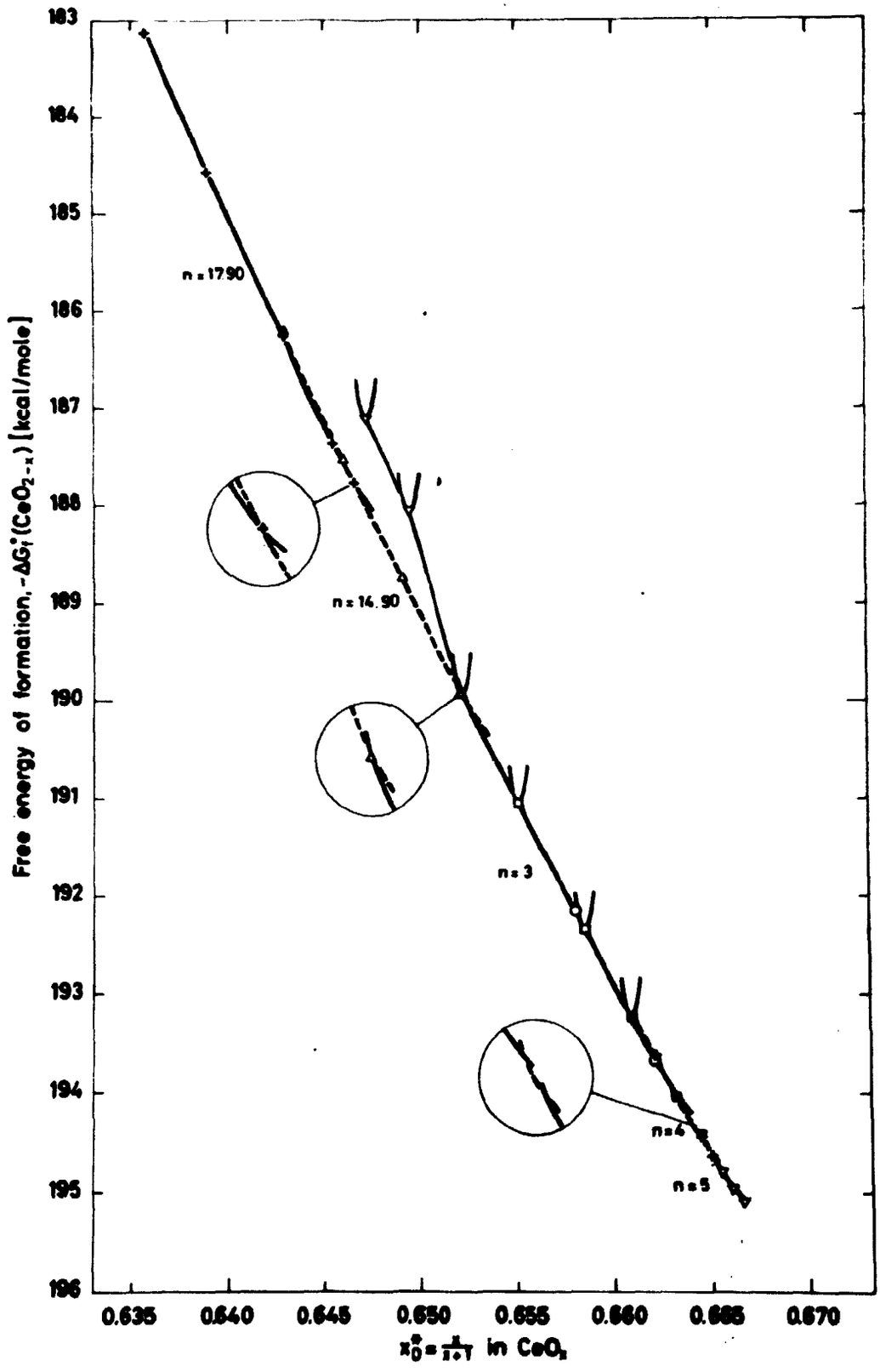

Fig. 8. Free energy of formation, $\Delta G_f^\circ(CeO_{2-x})$, of the subregions at 1000°C as a function of the mole fraction of oxygen, x°.

log x plot clearly indicates the possibility of ordered discrete phases, and the free energies of formation for these compounds are also indicated in fig. 8. The two-phase regions between the discrete phases must in this case be drawn as a common tangent between the free energy curves. But, as shown in the figure, these tangents practically coincide with the smooth curve found when the subregion was considered as non-stoichiometric, and the free energy changes accompanied by ordering must be small for the cerium oxides. The $\Delta G_f^o(CeO_{2-x})$ for the possible discrete compounds in the n = 14.90 subregion is also indicated in the figure. In this case, however, the curve obtained when the region is considered non-stoichiometric lies well below the common tangents between the free energy curves for the discrete phases, and these phases are apparently metastable at 1000°C.

2.4. High Temperature X-Ray Diffraction: Experimental

2.4.1. Equipment and Technique

The high temperature X-ray diffraction measurements were carried out in a Philips high temperature diffractometry attachment, shown in fig. 9. In this equipment, the powdered sample is placed in a small tantalum boat supported on a tungsten rod located in the centre of a small furnace made from molybdenum foils. Finally this furnace is placed in a vacuum chamber equipped with beryllium windows. The sample temperatures can be measured with a tungsten/tungsten, rhenium thermocouple placed in a hole in the supporting rod below the sample holder. In this arrangement, where the X-rays are passed to the sample through a slit in the heating element and in the surrounding heat shield, these temperatures cannot be considered as representative sample temperatures because of the severe radiant heat loss especially from the sample surface where the actual X-ray measurements are made. In order to determine the actual sample temperatures, ThO_2 was used as an internal calibrant, since its lattice parameter is known as a function of temperature and its diffraction peaks are well separated from the cubic CeO_2 peaks. For reliable measurements it is, of course, necessary that the ThO_2 does not react with the cerium oxides, but even at the highest temperatures used in this investigation (actual: 855°C), sharp ThO_2 peaks were obtained indicating that this reaction is not important in these measurements.

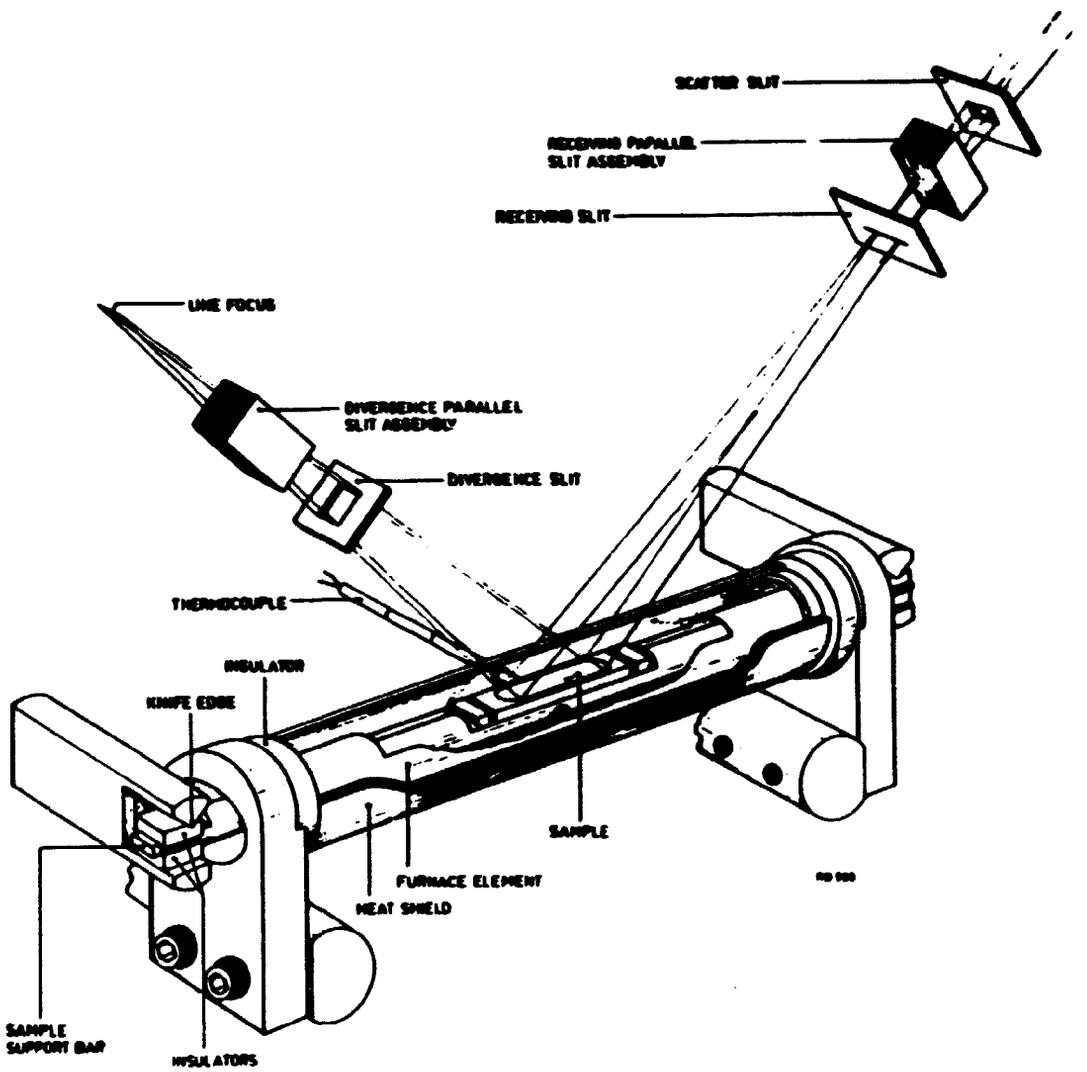

Fig. 9. Principle of Philips high temperature X-ray diffractometer.

2.4.2. Calculations

The lattice parameters for ThO_2 and CeO_2 and their respective standard deviations were obtained in a least square refinement by a computer program developed by Brown (39). The actual temperatures were determined from the lattice parameters of ThO_2, which had previously been determined as a function of temperature by Brown and Chitty (40) and Hock and Momin (41).

2.5. High Temperature X-Ray Diffraction: Results and Discussion

2.5.1. Lattice Expansion with Temperature

Previously Brauer and Gingerich (16) have shown that the lattice parameter of CeO_2 varies linearly with temperature up to 900°C. This was also confirmed in the present investigation as shown in fig. 10, where the results from both investigations are shown as a function of temperature.

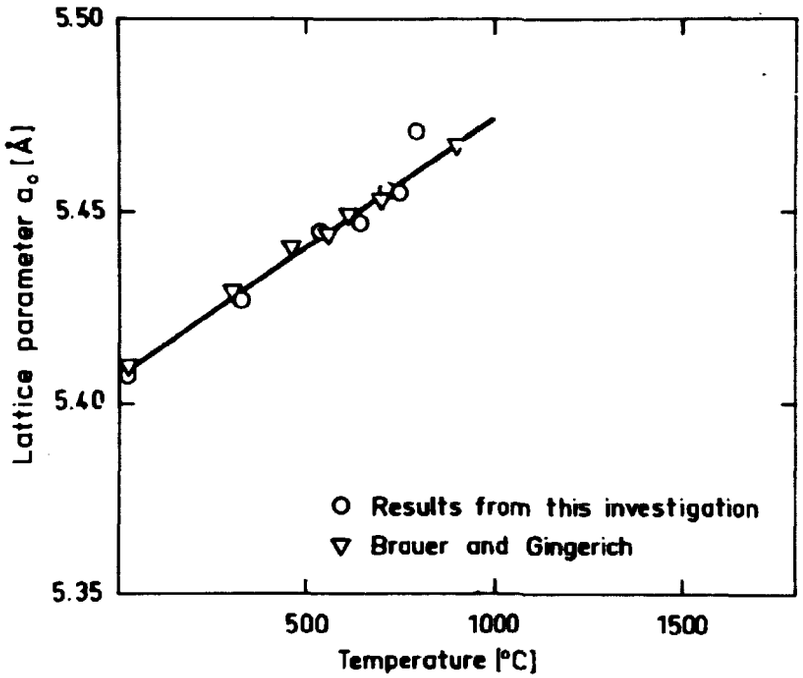

Fig. 10. Lattice parameter of CeO_2 as a function of temperature.

From the figure it will be noted that the agreement between the two sets of data is excellent. Unfortunately, the composition of the samples in the present investigation is not known precisely. However, as the oxygen pressure of the vacuum employed is not sufficiently low for a substantial reduction to take place at low temperatures, it is assumed that the compositions up to an actual temperature of 750°C are very close to the stoichiometric composition. This is also confirmed by the shape of the X-ray peaks, which were sharp and well defined and showed no significant rhombohedral splitting of the fluorite peaks such as the presence of the rhombohedral β-phase, for instance, should give.

2.5.2. Formation of Superstructures

At 790°C the fluorite CeO_2 peaks are still present although weak, but in the 855°C experiment these peaks were entirely absent. With the dis-

appearance of the fluorite structure another phase with many peaks was observed indicating the formation of a new structure of low symmetry. It was impossible to index the reflections for this phase under the assumption that the structure was of rhombohedral symmetry, which is closely related to the fluorite structure and which has been observed for many of the intermediate phases in the Ce-O system at lower temperatures. The great number of peaks indicates low symmetry, and indexing was tried under the assumption that the new structure was of triclinic symmetry, as reported by Sawyer et al. (42) for the ordered phases in the Pr-O system, but this also proved to be difficult. However, assuming that the structure is monoclinic with a unit cell similar to the monoclinic cell (space group $P2_1/n$, C_{2h}^5, found for $PrO_{1.833}$ (Pr_6O_{11}) by Lowenstein et al. (43) by single crystal methods, it was possible to account for all the reflections. The observed and calculated $\sin^2\theta$, as well as the indices for the different reflections are given in table 1.

Table 1

Powder pattern for monoclinic superstructure (space group: $P2_1/n$, C_{2h}^5) recorded by high temperature X-ray diffractometer at 855°C

Intensities[a]	d_{obs}(Å)	hkl	$\sin^2\theta_{obs}$	$\sin^2\theta_{calc}$
5	3.4659	121	0.0492	0.0490
2	3.3843	$\bar{1}31$	0.0516	0.0511
2	3.3223	$\bar{7}02$	0.0535	0.0532
2	3.2328	004	0.0565	0.0566
2	3.2224	$\bar{1}30$	0.0569	0.0567
3	3.2017	$\bar{7}04$	0.0576	0.0578
1	3.0300	$\bar{1}15$	0.0644	0.0645
1	3.0141	$\bar{7}11$	0.0651	0.0658
2	2.9641	040	0.0673	0.0671
1	2.7958	$\bar{1}34$	0.0756	0.0757
2	2.7726	200	0.0769	0.0770
3	2.4469	043	0.0988	0.0989
3	2.4362	201	0.0997	0.0995
1	2.3913	211	0.1034	0.1037
4	2.2456	133	0.1173	0.1172
1	2.2736	230	0.1144	0.1147
1	1.9732	$\bar{3}11$	0.1520	0.1525
2	1.9684	$\bar{3}34$	0.1527	0.1539
3	1.9597	061	0.1541	0.1545
2	1.7371	242	0.1962	0.1961
2	1.7304	$\bar{3}42$	0.1977	0.1976
1	1.7084	$\bar{7}63$	0.2029	0.2030
2	1.6746	037	0.2112	0.2110
1	1.5875	$\bar{3}56$	0.2350	0.2349
1	1.5497	$\bar{5}02$	0.2466	0.2463
1	1.5445	312	0.2483	0.2484

[a] Visually estimated on a scale from 1 to 5.

A least square calculation gives the following lattice parameters and their standard deviations for this unit cell at 855°C:

$a_o = 6.781 \pm 0.006$ Å

$b_o = 11.893 \pm 0.009$ Å

$c_o = 15.823 \pm 0.015$ Å

$\beta = 125.04 \pm 0.04°$.

These parameters correspond closely to the lattice parameters reported for the monoclinic $PrO_{1.833}$ (Pr_6O_{11}) cell, which Lowenstein et al. have shown can be derived from twelve fluorite cells. Although very little reduction of the samples apparently took place at lower temperatures, some reduction must be expected with increasing temperature where the sample holder (Ta) and furnace heating element (Mo) can act as oxygen getters. The thermogravimetric measurements also indicated the possibility of an intermediate phase with the composition Ce_6O_{11}, and obviously this phase was obtained in the high temperature X-ray measurements.

Several models have been proposed in order to describe the structures of the ordered intermediate phases. Hyde et al. (34), for instance, proposed that the structural entity, which generates the series M_nO_{2n-2}, is a linear infinite MO_6 string along the ⟨111⟩ directions surrounded by a contiguous sheath of MO_7. In Ce_7O_{12}, Ce_9O_{16} and $Ce_{11}O_{20}$ the strings are parallel and regularly spaced (42) whereas the strings run along all four ⟨111⟩ directions in the C-type oxide of Ce_2O_3 giving an ordered omission of 25% of the oxygen ions. Thornber et al. (35) subsequently suggested that the string model is incorrect and that the defects are clustered into units consisting of six seven-coordinate cations about one six-coordinate cation. Recently Martin (44) introduced the concept of octahedrally coordinated anion vacancies that gather on regularly spaced {213} planes. Whether the superstructures of the ordered intermediate phases can be described by these models, or whether they can be obtained by a crystallographic shearing mechanism, as proposed by Eyring and Holmberg (45), for instance, cannot be decided from the present results. Nevertheless the electron microscopy studies on reduced CeO_2 single crystals described in section 4 seem to indicate that the shearing mechanism plays an important role during the formation of these superstructures.

3. THERMODYNAMIC STUDIES OF THE PHASE RELATIONSHIPS IN NON-STOICHIOMETRIC PLUTONIUM AND URANIUM/PLUTONIUM OXIDES

In previous thermodynamic studies (46-50) of the Pu-O and U-Pu-O systems, the MO_{2-x} phase has always at higher temperatures been considered as a single grossly non-stoichiometric phase extending over a considerable composition range as shown in figs. 11 and 12, which give the accepted phase diagrams for the two systems.

As described in (5), thermodynamic data for these non-stoichiometric oxides were also determined by thermogravimetric analysis in the temperature range 900-1450°C in atmospheres of controlled oxygen pressures (CO_2/CO mixtures) using the same technique as for the CeO_{2-x} studies. A few high temperature X-ray diffraction measurements were also carried out in this part of the investigation mainly in order to study whether the superstructure ordering observed for the CeO_{2-x} oxides also takes place in a mixed oxyde system. Unfortunately it was, however, impossible to work with Pu-oxides in the equipment available for these studies and the X-ray measurements were therefore performed on mixed U/Ce-oxides.

3.1. Previous Studies

Previously the PuO_{2-x} system has been studied by Atlas and Schlehman (47, 48) by measurements of the electrical conductivity as a function of oxygen pressure and temperature in the temperature range 1045-1505°C. Using regression equations, straight lines for each temperature were drawn through all the data obtained in the whole composition range, and from the slopes of these lines it was concluded that the defects in PuO_{2-x} are predominantly interstitial Pu-ions. Similar to the CeO_{2-x} oxides, however, it is today generally believed that the cation lattice is very stable for the Pu-oxides too. This is also supported by the analysis of covalent and ionic radius of oxygen for these oxides by Blank (33), which shows it is difficult to remove the metal ions from their lattice sites to form interstitial ions in these oxides. Extensive thermodynamic data for the PuO_{2-x} system have also been determined by the emf technique by Markin et al. (46) in the temperature range 700-1140°C. The great change observed in enthalpy and entropy observed in this work when PuO_2 is reduced to $PuO_{1.75}$ was explained by the formation of coupled oxygen vacancies (grossly substoichiometric PuO_2) when the oxides were reduced substantially.

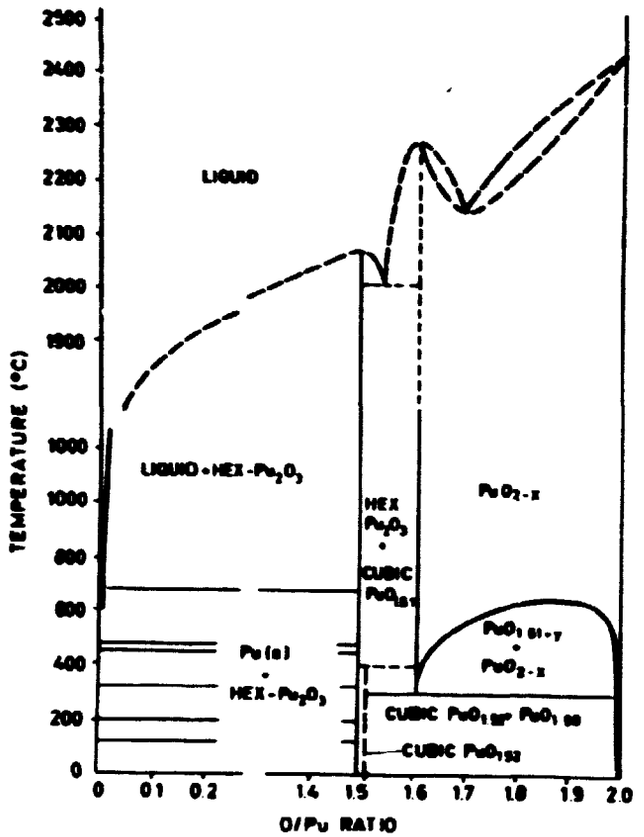

Fig. 11. Phase diagram for the Pu-O system.

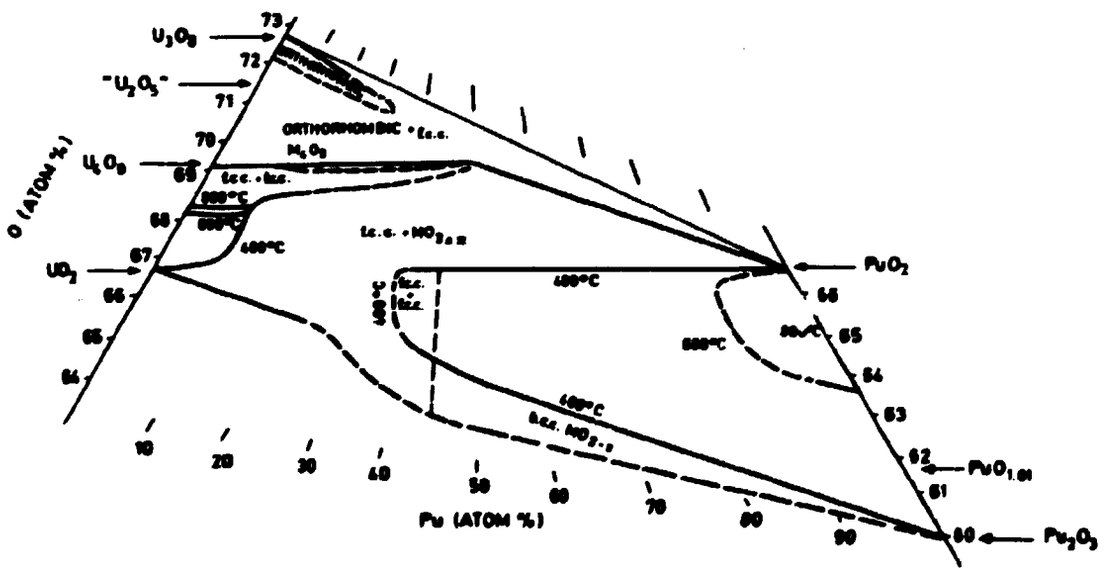

Fig. 12. Phase diagram for the U-Pu-O system.

Thermodynamic data on the mixed U/Pu-oxides have previously been determined by Woodley (50) by thermogravimetric analysis on $(U_{0.75}Pu_{0.25})O_{2-x}$ in H_2/H_2O mixtures in the temperature range 950-1400°C. The data obtained in this study compare well with Markin and McIver's data (49), which were determined by the emf technique in the temperature range 700-1140°C on oxides containing 10 and 30% Pu. These data show that the thermodynamic data for oxides in this composition range only depend on the valency of the Pu-ions and not on the Pu-content. The data published by Woodley and by Markin and McIver, however, show some disagreement with the data published by Javed (51) on $(U_{0.80}, Pu_{0.2})O_{2-x}$. The reason for this discrepancy can probably be explained by the more indirect method used by Javed in which the composition obtained during equilibration in H_2/H_2O mixtures at higher temperatures was determined after quenching the samples to room temperature. Much smaller changes in $\Delta\overline{H}_{O_2}$ with composition are observed for the mixed oxides than for PuO_{2-x}. This indicates that the Pu-ions must play a significant role, as suggested by Markin and Roberts (see (52)), who proposed that local ordering of the oxygen vacancies can only take place if a large fraction of reducible cations is present. This is also suggested in the statistical model recently proposed by Manes (32) for PuO_{2-x} and $(U, Pu)O_{2-x}$, which was already mentioned in section 2.3.1, where defect complexes consisting of at least one oxygen vacancy and two Pu-ions were considered.

The relative partial enthalpies, $\Delta\overline{H}_{O_2}$, have also been determined by microcalorimetric measurements for the PuO_{2-x} and $(U, Pu)O_{2\pm x}$ oxides by Chereau et al. (53) at 1100°C. Near the stoichiometric composition the $\Delta\overline{H}_{O_2}$ values obtained with this method compare well with the values published by Markin and McIver, but at a greater deviation from stoichiometry substantial disagreement between the two investigations was observed. The directly measured values are, however, more accurate than those calculated from $\Delta\overline{G}_{O_2}$ and the data obtained by Chereau et al. are probably the most correct.

3.2. Thermogravimetric Analysis: Experimental

3.2.1. Starting Material

The PuO_2 used in the thermogravimetric measurements was of nuclear grade of high purity, while the mixed U/Pu oxides were prepared by co-precipitation of ammonium diuranate and plutonium hydroxide from nitrate solutions. After filtration, the precipitates were calcined at 500°C in air and then reduced to stoichiometric composition in hydrogen at 1000°C.

3.2.2. Thermogravimetric Measurements

The thermogravimetric equilibrium measurements were carried out on PuO_2, $(U_{0.90}Pu_{0.10})O_2$ and $(U_{0.80}Pu_{0.20})O_2$ in atmospheres of controlled oxygen pressures (CO_2/CO mixtures) by continuous heating in the temperature range 900-1450°C. The experimental conditions used are given in table II.

Table II

Temperature range:	**900-1450°C**
Heating rate:	**20-900°C: 10°C/min**
	900-1450°C: 2°C/min
Cooling rate:	**1450-20°C: 10°C/min**
Atmospheres (CO_2/CO):	**1/1000 to 1/1**
Sample weight:	**500-800 mg**
Crucible:	**Al_2O_3**

The principle of the gas system for mixing CO and CO_2 for the Pu experiments was the same as that used in the CeO_{2-x} studies described in section 2.2.2. Also in these experiments the oxygen pressures of the atmospheres used were controlled by continuous measurements with a ZrO_2(CaO) cell. In the present case though the measurements were performed on the exit gas from the balance while the composition of the inlet gasses was controlled by frequent gas-chromatographic analysis. Pu-oxides are extremely poisonous materials to work with and the balance was therefore enclosed in a glove box during these studies. The glove box developed for this work is shown in fig. 13.

3.3. Thermogravimetric Analysis: Results and Discussion

3.3.1. Thermodynamic Data for PuO_{2-x}

The $\Delta\overline{G}_{O_2}$ values and the composition of the PuO_{2-x} samples, which were both calculated as described for the CeO_{2-x} studies, are shown in fig. 14 together with the data previously published by Atlas and Schlehman (47, 48) and Markin et al. (46).

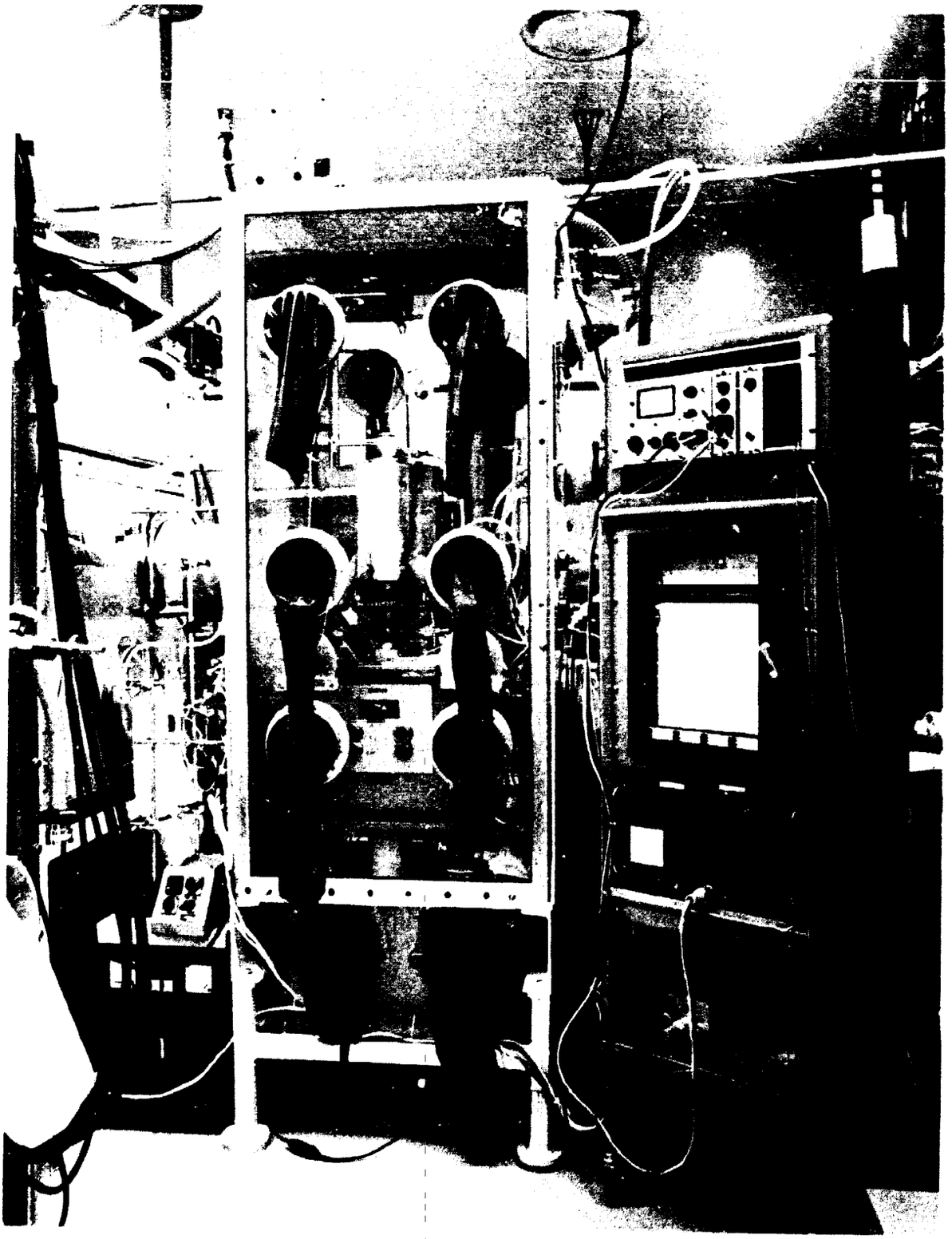

Fig. 13. Glove box arrangement for the thermogravimetric studies of PuO_{2-x} and $(U, Pu)O_{2-x}$.

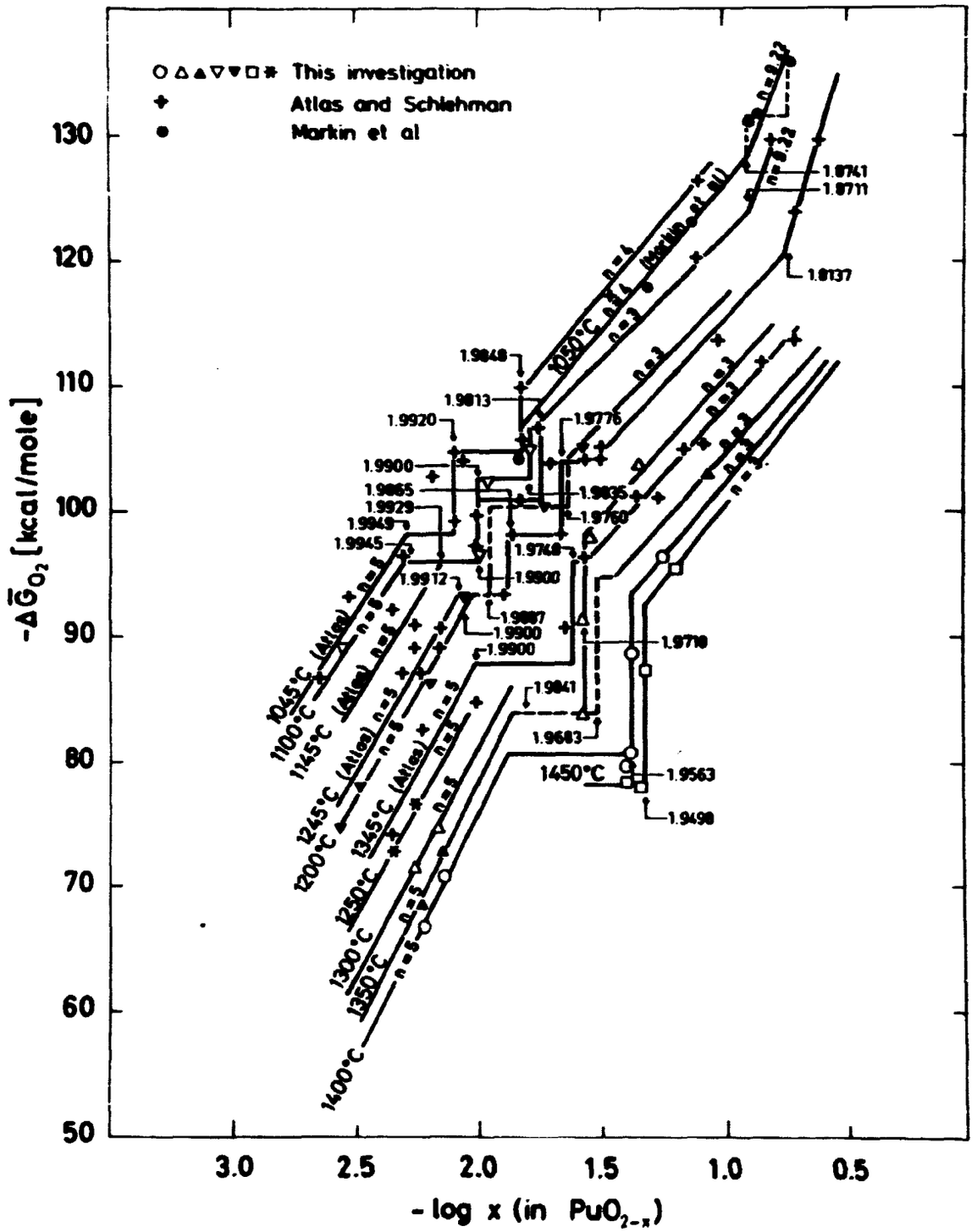

Fig. 14. Relative partial free energy of oxygen, $\Delta\bar{G}_{O_2}$, of PuO_{2-x} as a function of composition (log x).

Comparing the three data sets it will be noted in general that they show the same trend in the curves although some discrepancy exists between the $\Delta\bar{G}_{O_2}$ values. Generally the data reported by Atlas and Schlehman are slightly higher than both the $\Delta\bar{G}_{O_2}$ values obtained in the present investigation and those found by Markin et al. by the emf technique. One reason for this discrepancy could be the more accurate control of the oxygen activity that can be obtained by the emf technique, and which in the present investigation was obtained by frequent gas-chromatographic checks and by continuous control with the $ZrO_2(CaO)$ oxygen cell.

Considering all the data points in fig. 14 it is clear that the linear relationship between $\Delta\bar{G}_{O_2}$ and log x depicted in eq. (7) is also obtained within certain regions for the PuO_{2-x} oxides. Near the stoichiometric composition the slope of the lines corresponds to a value of n = 5, whereas at greater deviation from stoichiometry n = 4 at 1050°C and n = 3 at higher temperatures. Finally at substantial reductions n = 9.22 at least up to a temperature of ~1250°C. As observed for the CeO_{2-x} system the non-stoichiometric PuO_{2-x} phase can also be divided into subregions, which can each be described thermodynamically by a characteristic value of n, indicating that a characteristic defect is formed within each subregion. In principle the types of defect present in the different subregions can be evaluated from the values obtained for n, but as described for the CeO_{2-x} system this can only be rather speculative since the defect theories on which such an evaluation should be founded are based on assumptions that are probably not fulfilled - randomly distributed non-interacting defects. Atlas and Schlehman also observed slopes corresponding to n = 5 at lower temperatures which they interpreted in terms of interstitial Pu-ions. In their treatment, however, straight isotherms were drawn through all the data points obtained in the whole composition range by using regression equations, and information about the detailed nature of the PuO_{2-x} phase is obviously lost by this procedure. As shown in fig 14, the scatter of their experimental points is in fact substantially reduced if straight lines of varying slopes are drawn instead of a single line. Furthermore it is no longer believed that it is possible to form interstitial cations in these oxide systems, as explained previously (section 3.1), and the interpretation offered by Atlas and Schlehman is probably incorrect.

Considering the curves in fig. 14 in terms of the phase rule criteria for a binary oxide system in equilibrium with a gas phase, the following information about the phase relationship of the PuO_{2-x} system can be obtained:

(1) The subregions can be considered as consisting of apparently non-stoichiometric single phases whose macroscopic thermodynamic properties can be described by a characteristic value of n.

(2) Values of $n \leq 6$ can probably be taken as an indication of the presence of single defects or defect clusters, but this is not the case for $n = 9.22$ which is observed below $O/M = 1.875$. For the CeO_{2-x} system a clear indication of a series of discrete phases separated by two-phase regions was observed for the $n > 6$ subregions. The $n = 9.22$ subregion observed for the PuO_{2-x} system can probably be interpreted in a similar way (see Markin's data in fig. 13).

(3) Near the stoichiometric composition the data strongly indicate the existence of discrete phases and two two-phase regions. These phases have not been observed in previous studies of this system.

If the compositions for the discrete phase, the two-phase regions and the subregion boundaries are plotted as a function of temperature, the T, x diagram shown in fig. 15 is obtained.

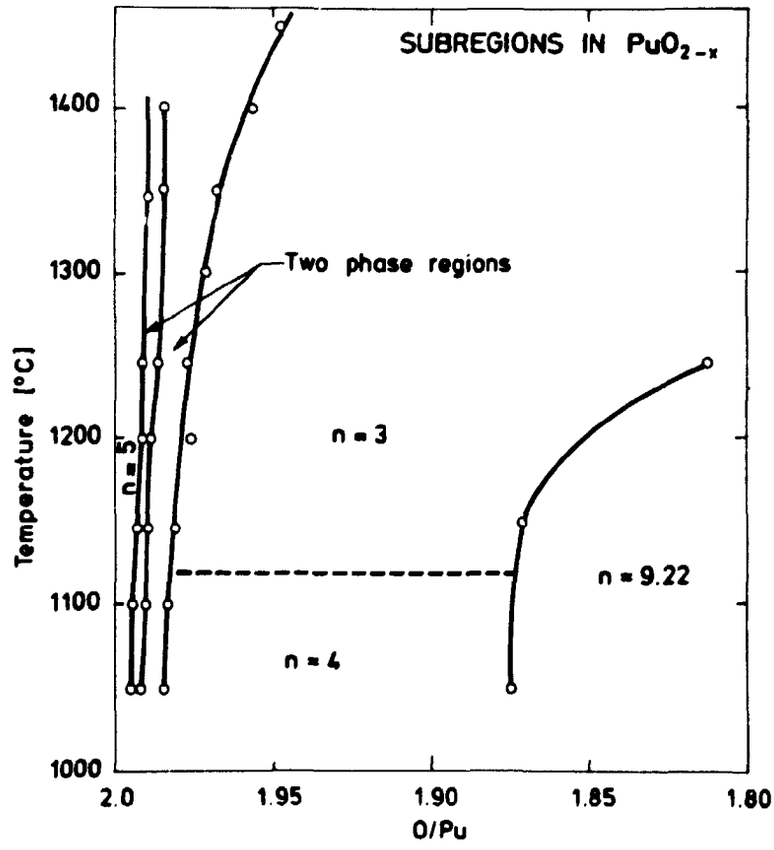

Fig. 15. Diagram of subregions for PuO_{2-x}.

The diagram again clearly demonstrates that the PuO_{2-x} phase field can be divided into subregions, some of which are non-stoichiometric ($n \neq 5$), or probably consist of a series of discrete phases ($n = 9.22$), and some of which are two-phase regions. Compared to the T, x diagram for the CeO_{2-x} system shown in fig. 4, it will be noted that the pattern of subregions for the PuO_{2-x} system apparently is somewhat different from that of the CeO_{2-x} system. Before the subregion pattern for the PuO_{2-x} system can be finally established, however, much more data should be available, and thus the T, x diagram shown in fig. 15 can only be considered as preliminary. It is also interesting to compare the composition observed for the subregion boundaries in this work with the limits found in Manes's statistical calculations - O/M = 1.91; 1.83; 1.74, and 1.65 (see section 2.3.1). As in the case of the CeO_{2-x} system, no boundary at O/M = 1.91 was observed for the PuO_{2-x} system, whereas the boundary between the n = 3 and n = 9.22 subregions only passes through O/M = 1.83 at higher temperatures. The agreement between the present results and those predicted by Manes' statistical model is thus not very convincing. Perhaps this discrepancy can be explained by the formation near the stoichiometric composition of the discrete-ordered phase, which cannot be predicted by the statistical model.

As explained for CeO_{2-x}, $\Delta\overline{G}_{O_2}$ should vary linearly with temperature for constant composition within the non-stoichiometric subregions if this treatment is valid. From the $\Delta\overline{G}_{O_2}$ versus temperature curves obtained for the compositions (2-x) = 1.9960 and (2-x) = 1.9498 in fig. 16, it will be noted that this linear relationship is also obtained for the n = 5 and 3 regions in the PuO_{2-x} system.

Using eqs. (3) and (4) (section 2.2.4), $\Delta\overline{S}_{O_2}$ and $\Delta\overline{H}_{O_2}$ were calculated from these lines, and the results obtained are shown in table III together with data calculated from Atlas and Schlehman's results. The data previously published by Markin et al., and those obtained by Chereau et al. by microcalorimetric measurements at 1100°C, are also given in this table.

Table III

Composition (2-x)	n	$-\Delta\bar{S}_{O_2}$ (eu)	$-\Delta\bar{H}_{O_2}$ (kcal/mole)	Comments
1.9960	5	121	258[x]	This work
1.9960	5	69	185.95[x]	Atlas and Schlehman (47, 48)
~ 1.9960		~ 125	259	Markin et al. (46)
~ 1.9960			256	Chereau et al. (53)
1.9498	3	87.5	240.15[x]	This work
1.9498	3	72.5	216.65[x]	Atlas and Schlehman
~ 1.950		90	239	Markin et al.
~ 1.950			241	Chereau et al.

[x] calculated at 1100°C

From the table it is clear that the $\Delta\bar{H}_{O_2}$ and $\Delta\bar{S}_{O_2}$ values obtained in the present investigation closely agree both with the data of Markin et al. and with those of Chereau et al., whereas the values calculated from Atlas and Schlehman's experimental points are apparently too high. This is also the case with the values they obtained in their original treatment, where all points obtained at one temperature were considered to belong to the same regression line, and where they obtained $\Delta\bar{H}_{O_2}$ = - 192 and - 225 kcal/mole for $PuO_{1.99}$ and $PuO_{1.95}$ respectively.

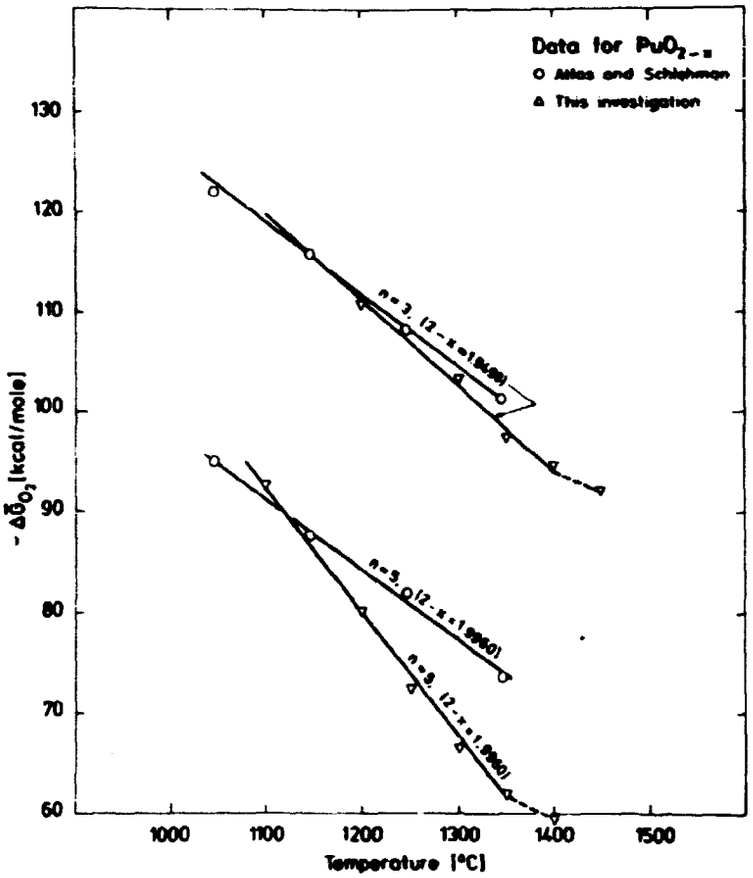

Fig. 16. Relative partial free energy of oxygen, $\Delta\bar{G}_{O_2}$, of PuO_{2-x} as a function of temperature for constant composition.

3.3.2. Thermodynamic Data for $(U, Pu)O_{2-x}$

The data obtained in the thermogravimetric equilibration measurements, which were carried out on $(U_{0.9}Pu_{0.1})O_{2-x}$ and $(U_{0.8}Pu_{0.2})O_{2-x}$, were treated in the same way as the PuO_{2-x} data. The results are shown in fig. 17, where the $\Delta\bar{G}_{O_2}$ values at each temperature are plotted as a function of log x together with thermogravimetric data recently published by Woodley (50) for $(U_{0.75}Pu_{0.25})O_{2-x}$.

Because of the great stability of the mixed oxides, only a rather limited composition range could be covered with the gas mixtures used in the present investigation. Nevertheless, it is clear from the figure that the present results closely agree with Woodley's results, which again show good agreement (see Woodley's paper) with the data obtained by Markin and McIver (49) by the emf technique in the temperature range 700°C to 1140°C.

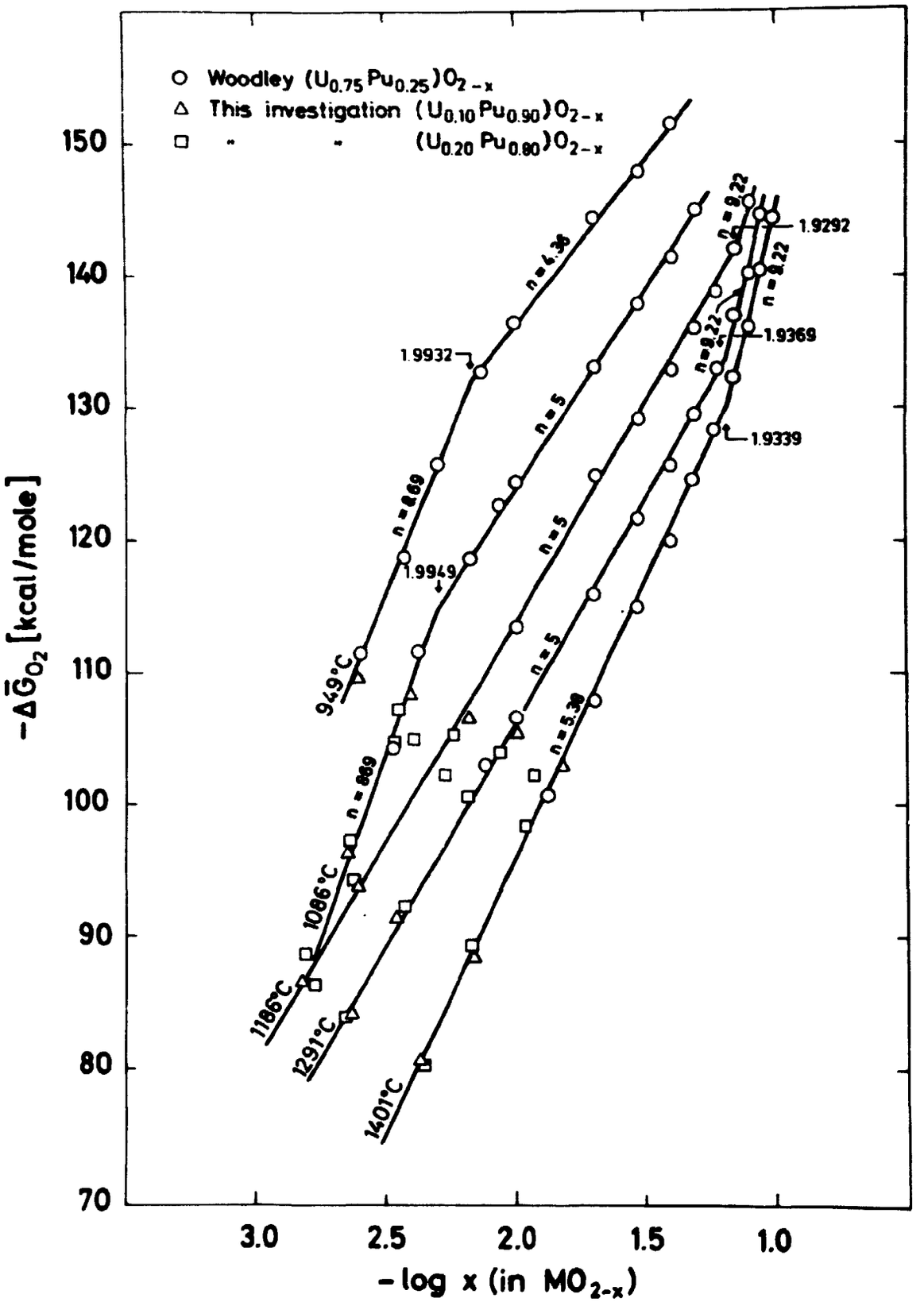

Fig. 17. Relative partial free energy of oxygen, $\Delta\bar{G}_{O_2}$, of $(U, Pu)O_{2-x}$ as a function of composition (log x).

Considering all the data points in fig. 17, it will be noted that the linear relationship predicted by the defect theories is also obtained with mixed oxides. For the two oxides investigated it is clear that the sub-stoichiometric range can also in this case be divided into several subregions corresponding to the different slopes of the straight lines. Near the stoichiometric composition at lower temperature, for instance, a subregion corresponding to n = 8.69 is obtained, whereas regions with n = 5; 4.36 (at lower temperature) and 9.22 are obtained at greater deviations from stoichiometry. As explained for the CeO_{2-x} and PuO_{2-x} systems, the n = 5 values can be explained by the presence of single defects or defect clusters, whereas higher values of n probably indicate the existence of a continuous sequence of discrete phases separated by two-phase regions. The n = 9.22 region was also observed for the PuO_{2-x} system, but the n = 8.69 region at small x is apparently only present in the mixed oxides. Whether this region really consists of discrete phases is, of course, for the present a matter for consideration, but a close examination of the single experimental points published by Markin and McIver certainly indicates the possibility of a two-phase region near the stoichiometric composition (see fig. 14 in (52); $\Delta\overline{G}_{O_2}$ versus O/M for $(U_{0.89}Pu_{0.11})O_{2\pm x}$).

The T, x diagram obtained for the mixed oxides is shown in fig. 18. Compared to the PuO_{2-x} system (fig. 15), the two-phase ranges between the n = 5 and n = 3 subregions are apparently not formed in the mixed oxides indicating that ordering reactions of the defects are much more difficult in these oxide systems. The n = 5 region, in which single defects or simple defect clusters are probably formed, also extends to much lower O/M values for the mixed oxides than for PuO_{2-x} which is also an indication of the greater stability of the defect structure in mixed oxides. Another difference between the two oxide systems is that where the nature of the defects in the PuO_{2-x} oxides can apparently change in several steps before reaching the n = 9.22 subregion with a continuous sequence of discrete phases - only one type of defect is observed for the mixed oxides. In addition it seems that the PuO_{2-x} oxides are more reactive than the mixed oxides, probably because of the greater amount of Pu-ions. Markin and Roberts proposed that these play an important role during defect ordering reactions.

Straight $\Delta\overline{G}_{O_2}$ versus temperature lines were also observed for the mixed oxides at constant composition for each of the subregions as shown in fig. 19 and in table IV, the $\Delta\overline{H}_{O_2}$ values calculated from these lines compare well with Chereau's microcalorimetric data (53).

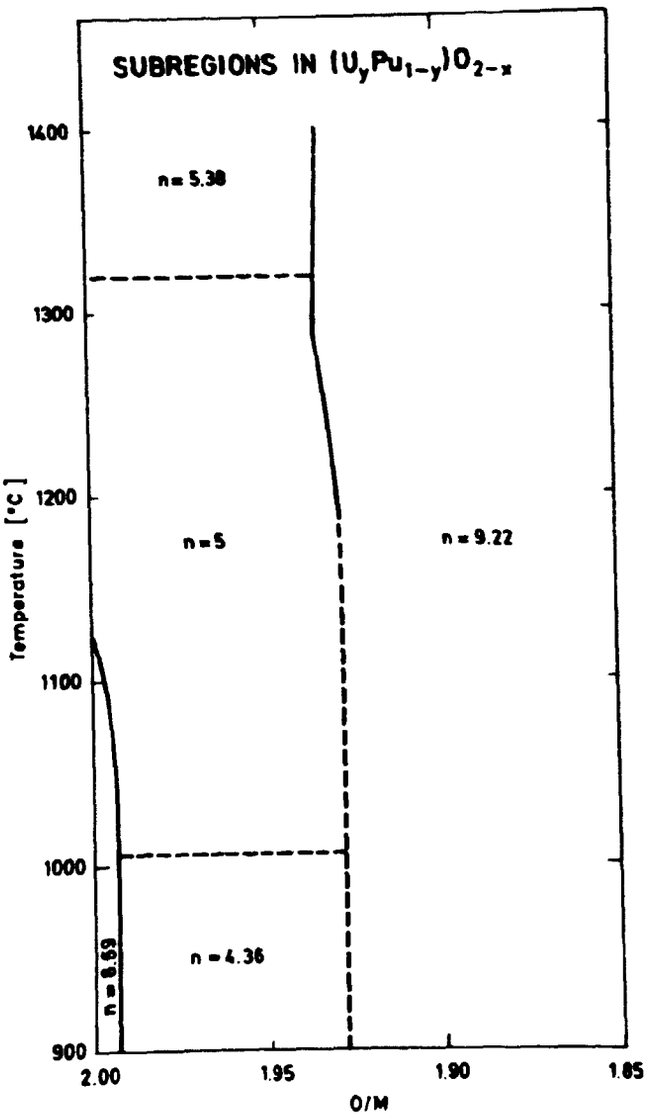

Fig. 18. Diagram of subregions for $(U, Pu)O_{2-x}$.

Table IV

Composition (2-x)	n	$-\Delta\bar{S}_{O_2}$ (eu)	$-\Delta\bar{H}_{O_2}$ (kcal/mole)	Comments
1.9968	8.69	90	226.18[x]	This work
1.9950			~225	Chereau et al.
1.9950		~52	~190	Markin and McIver
1.9900	5	86.9	241.91[x]	This work
1.9900			~235	Chereau et al.
1.9900		~50	~192	Markin and McIver

[x] calculated at 1100°C

The table also shows the $\Delta\overline{S}_{O_2}$ values calculated from the $\Delta\overline{G}_{O_2}$ versus temperature lines in the present work, as well as the data previously published by Markin and McIver. Apparently there is some disagreement between the two data sets, but as the present $\Delta\overline{H}_{O_2}$ values correspond closely to the microcalorimetric values, Markin and McIver's data are probably too high.

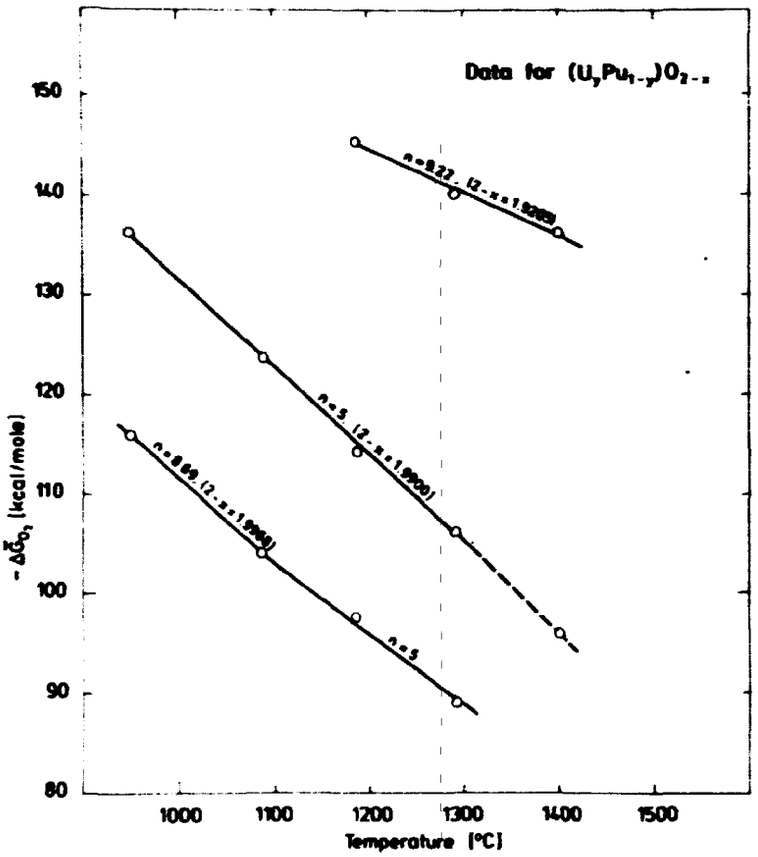

Fig. 19. Relative partial free energy of oxygen, $\Delta\overline{G}_{O_2}$, for $(U, Pu)O_{2-x}$ as a function of temperature for constant composition.

3.4. High Temperature X-Ray Diffraction: Experimental

3.4.1. Starting Materials

The X-ray measurements were carried out on the mixed oxides $(U_{0.9}Ce_{0.1})O_2$ and $(U_{0.8}Ce_{0.2})O_2$, which were prepared by coprecipitation of ammonium diuranate and cerium hydroxide from nitrate solutions. Similar to the mixed $(U, Pu)O_2$, the precipitates were also calcined at 500°C in air and then reduced in hydrogen at 1000°C in order to obtain the stoichiometric composition.

3.4.2. Equipment and Procedures

The equipment and the procedures described for the X-ray measurements on CeO_2 were also used for the mixed oxides. The temperature range covered in these measurements was 25-875°C.

3.5. High Temperature X-Ray Diffraction: Results and Discussions

The cubic lattice parameter calculated by a least square refinement for the two oxides showed good agreement with the results previously published by Markin and Street (54) for the U-Ce-O system, and the actual results obtained will not be repeated here. Contrary to the splitting of the peaks due to superstructure formation observed for CeO_{2-x}, all peaks for the mixed oxides were sharp and well defined, and there was no sign of extra peaks at higher temperatures indicating a change in structure. The mixed oxides thus seem to be more stable than the pure oxides, as also indicated by the thermodynamic investigations.

4. ELECTRON MICROSCOPY STUDIES ON REDUCED CeO_2 SINGLE CRYSTALS

The thermogravimetric technique used in the thermodynamic studies described in the previous sections is only an indirect method, and in order to verify the existence of some of the intermediate phases observed in these studies some preliminary electron microscopy examinations of reduced CeO_2 single crystals were also carried out. In recent studies, especially on transition metal oxides, high resolution electron microscopy has proved to be a very useful technique. In fact, these studies have shown that the non-stoichiometric oxides can no longer be considered as grossly non-stoichiometric phases with a large concentration of defects or defect clusters, as assumed in the classical defect theories, but that an extensive crystallographic shearing takes place eleminating the defects. The majority of the previous electron microscopic studies were performed on oxides of the cubic ReO_3-type structure - see, for instance, the review by Eyring and Tai (55) and by Tilley (56) - and on oxides based on the rutile structure, e.g. Bursill and Hyde (7); but only little electron microscopy has been done hitherto on oxides with the fluorite or fluorite-related structures as found in the oxide systems examined in the present work.

For the TiO_x system, Merritt et al. (37) showed that the thermodynamic findings can be correlated quite closely with the structural behaviour observed by electron microscopy. This is a very important achievement, which is also the final goal for the oxide systems considered in the present work. However, this requires a far more detailed electron microscopy study than was performed during the present work, which can only by considered as preliminary and which can only indicate some of the possibilities for structural arrangements in these oxide systems. Nevertheless, the results described in this thesis,together with those recently obtained by Kunzmann and Eyring (57) in their electron microscopy studies on the Pr-O and Tb-O systems, show that electron microscopy is certainly of great value, also in studies of fluorite-related oxides. Further examinations using this technique thus appear to be particularly fertile for future research.

4.1. Experimental

4.1.1. CeO_2 Single Crystals

The CeO_2 single crystals were obtained from Imperial College, London, where they were grown in a PbF_2 melt from reagent grade ceria. After

receipt, the lattice parameter of the crystals was checked by X-ray diffraction analysis and found to be $a_o = 5.4117 \pm 0.0005$ Å, corresponding to the lattice parameter for stoichiometric CeO_2 (11).

4.1.2. Reduction of the Crystals

Two methods were used to reduce the single crystals:

(1) Heating with the electron beam in the microscope by removing the condenser aperture and concentrating the beam. The temperatures and thus the composition obtained in the particles is, of course, unknown when using this method, but it has the advantage of avoiding reoxidation of the reduced samples.

(2) Heat treatment in a vacuum furnace at a pressure of 3×10^{-6} mm Hg at 1440°C for 125 h. After this heat treatment the sample was quenched to room temperature (cooling time ~ 1 h). In order to avoid reoxidation, the crystals were kept in CCl_4 after the heat treatment. The conditions for this treatment give $\Delta\bar{G}_{O_2} = -77.33$ Kcal/mole, corresponding to a composition of $\sim CeO_{1.80}$ (n = 17.90 region).

4.1.3. Electron Microscopy Examination

The samples for the electron microscope were prepared by grinding the crystals in an agate mortar and then collecting the fine particles on a holey-carbon supporting film. The examination was carried out on a JEM-100C microscope equipped with a double-tilting side-entry goniometer ($\pm 45°$ both on x and y). A resolution of 3.5 Å can be obtained with this goniometer and the maximum magnification is 250,000 x.

Extensive use was made of selected area diffraction combined with dark-field microscopy. Through a combination of the two techniques it is possible to reveal which regions of the particles contribute to the different diffracted beams. Thus it is possible to determine, for instance, whether a spot observed on the diffraction pattern originates from a second particle (superposition of patterns) or from a special phase or region within the particle itself. In order to minimize the effect of spherical aberation on the resolution of the dark-field images, the illuminating system of the microscope was tilted in the dark-field mode so that the spot under examination was moved to the centre of the screen. This corresponds to the diffracted beam passing along the objective axis of the microscope. The lattice image technique was also tried, but unfortunately the particles giving suitable patterns (superstructure patterns) were all too thick to give lattice

image pictures. Provided that suitable particles can be found, however, there is no doubt that this technique can also be successfully applied to this oxide system in our microscope, because beautiful lattice, image pictures (fig. 20) were obtained during some preliminary examinations on Nb_3O_7 crystals (60).

Fig. 20. Lattice image electron micrograph of a Nb_3O_7F crystal showing lattice planes with regular spacings interrupted by defect structures with irregular spacings.

4.2. Observations Made on Beam-Heated Particles

4.2.1. Crystallographic Shearing

A typical diffraction pattern taken on a beam-heated particle is shown in fig. 21 together with a bright-field and a dark-field image and a standard stereographic projection on (111). In order to make the trace analysis as accurate as possible, this pattern was taken with the electron beam approximately perpendicular to the surface of the particle (x and y tilt equal to zero) (see Hirsch et al. (59)). The rotation of the images relative to the diffraction pattern, which was determined on a MoO_3 specimen to be 38^o with the camera length and the magnification used, is also taken into account as shown in fig. 21.

The pattern obtained is clearly a (111) pattern and the indices of the nearest spots are shown in the standard stereographic projection.

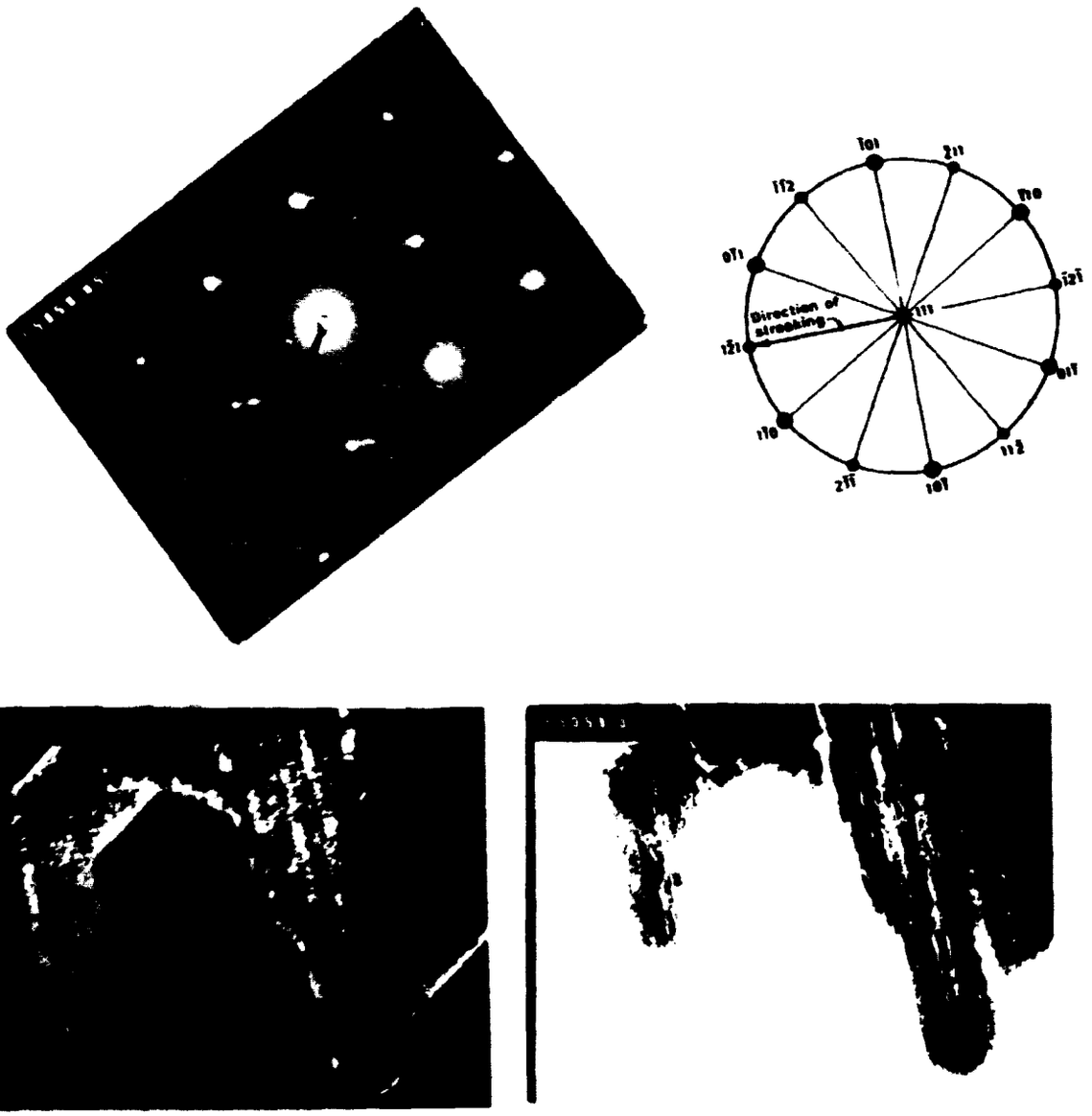

Fig. 21. Diffraction pattern, dark-field and bright-field images (mag. 50,000 x) of beam-heated particle showing streaks in the $[1\bar{2}1]$ direction. The indices of the spots on the diffraction pattern are shown on the stereographic projection. Note the fine structure perpendicular to the lamellae structure.

From the figure it is also clear that the pattern shows streaks in the $(1\bar{2}1)$ direction, which in some cases are split into separate spots. Comparing the dark-field image with the diffraction pattern, it will be noted that the particle shows traces of a lamellae structure lying perpendicular to the streaks, and apparently thin slabs parallel to the $(1\bar{2}1)$ planes form during the heat treatment in the beam. The $(1\bar{2}1)$ planes are perpendicular to the (111) plane, which for this particle is parallel to the surface of the particle as shown above; but the traces observed in the dark-field images could also originate from an inclined plane. Diffraction patterns taken on the same particle after tilting, as well as on other beam-heated particles (fig. 22), however, also show streaks which can be explained in all cases by the formation of a lamellae structure parallel to the $\{1\bar{2}1\}$ family of planes.

Tentatively it is proposed that the observed structure is formed by a crystallographic shearing mechanism. As can be seen in fig. 23a, which shows the oxygen and metal positions projected onto the (111) plane, a lamellae structure can be envisaged to form if the oxygen vacancies are ordered into a C-layer of oxygen atoms, and the structure then collapses if the oxygen atoms in adjacent layers jump into the vacant oxygen positions. In this way the metal atoms will move to an empty cube below the projection plane. Instead of cubes sharing edges in the normal fluorite structure, a structure with cubes sharing faces - which explains the decrease in the O/M-ratio - will be formed across the shear plane. The (111) projection is not suited for showing this mechanism, and in fig. 23b the projection is made on the $(10\bar{1})$ plane that is perpendicular to the $(1\bar{2}1)$ plane. This projection, which is different from that used by Hyde (60) in his proposal of a crystallographic shearing mechanism in oxides of fluorite structure, clearly shows the formation of a thin slab by the mechanism described above.

Different models have been proposed for the reduction of ReO_3-type crystals by crystallographic shearing - Gado (61), Anderson and Hyde (62), Andersson and Wadsley (63), and Van Landuyt and Amelinckx (64). Whether the shear planes in the fluorite structures are formed by growing dislocation loops, as proposed by Anderson and Hyde, or by co-operative migration of cation planes, as proposed by Andersson and Wadsley, cannot of course be decided on the basis of the present results. However, the mechanism shown in figs. 23 a and b seems to involve the co-operative migration of the Andersson/Wadsley model.

Recently the concept of swinging shear planes was introduced by Bursill and Hyde (7) in their studies of the TiO_x system. For this system it was observed that the orientation of the shear planes changed in an intermediate

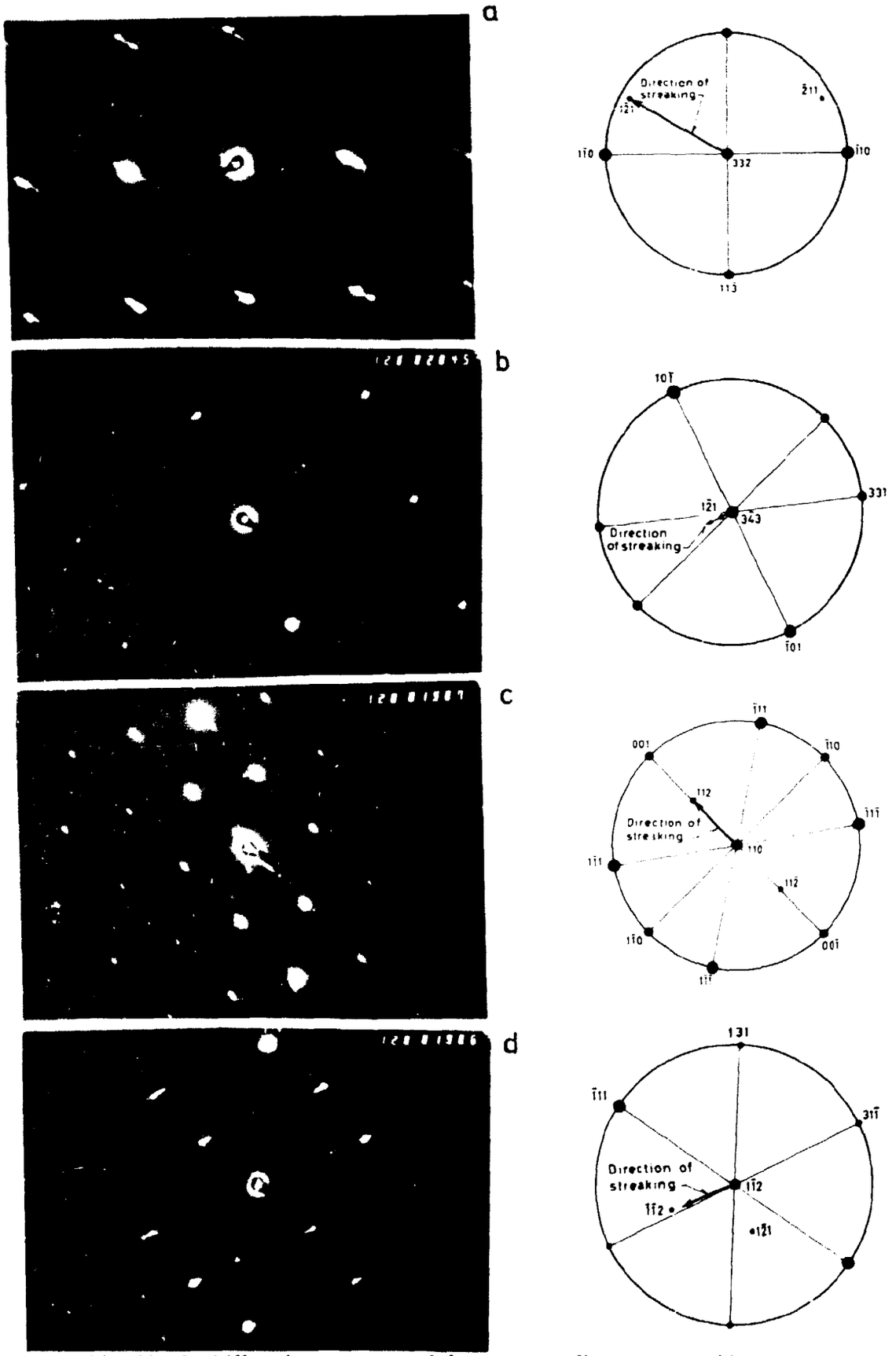

Fig. 22a-d. Diffraction patterns and the corresponding stereographic projections taken on beam-heated particles - a) and b) were taken on the same particle as shown in fig. 19 but in other directions; c) and d) were taken on other particles.

phase range in which very little hysteresis was found. The thermodynamic studies described in the previous sections showed amazingly little hysteresis for the CeO_2 system, and this concept should also be considered in further studies of crystallographic shearing in the fluorite-related oxides.

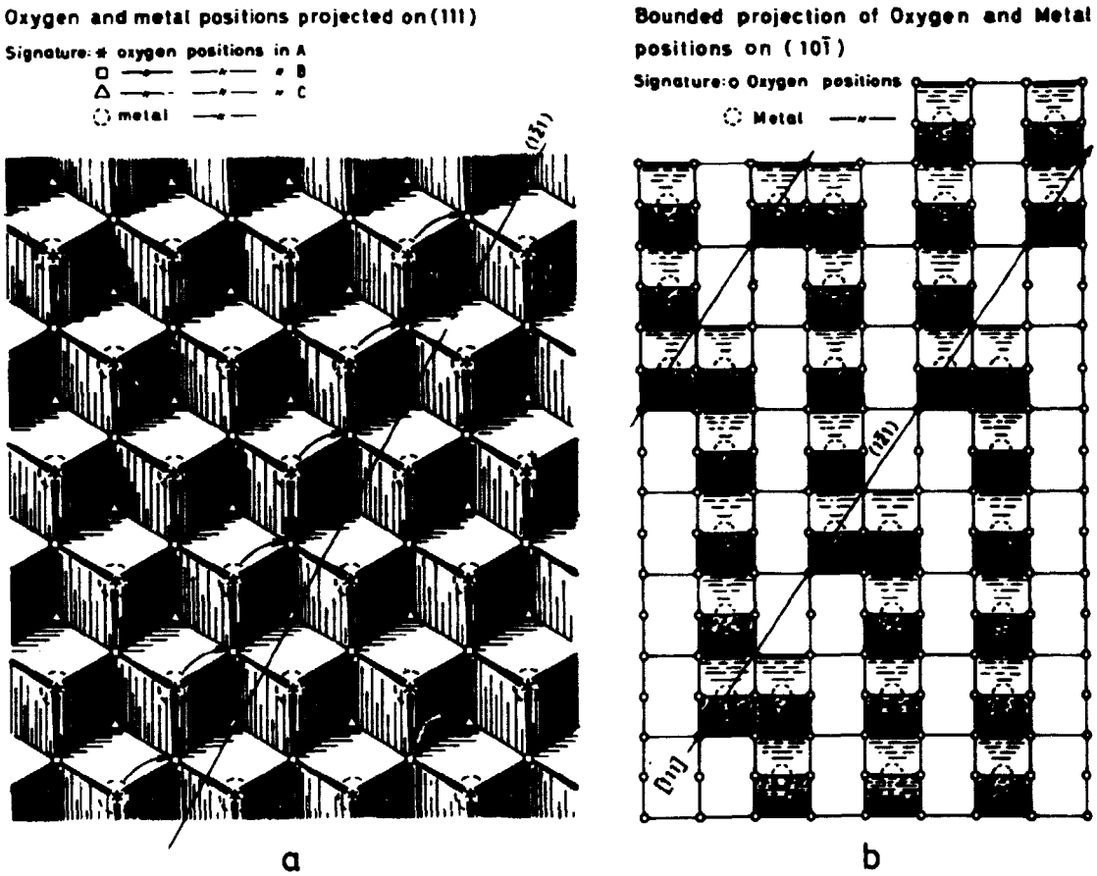

Fig. 23a and b. Oxygen and metal atoms projected on to (111) and (10$\bar{1}$) respectively, showing crystallographic shearing along (1$\bar{2}$1). The formation of a thin slab parallel to (1$\bar{2}$1) is shown in b.

4.2.2. Superstructure Patterns

In some of the beam-heated particles the superstructure pattern shown in fig. 24 was observed.

For the CeO_{2-x} system, the high-temperature X-ray diffraction analysis showed that monoclinic superstructures can be formed at higher temperatures. As shown in fig. 24, it was possible to index the observed pattern assuming that this structure was formed during the beam heating. Similar superstructure patterns have also been reported by Kunzmann and Eyring (57) for the Pr-O and Tb-O systems, and ordering of the defects into superstructures is apparently a general mechanism for the fluorite-related oxides. In the model for crystallographic shearing in ReO_3-type oxides by Gado (61), a superstructure can be assumed to precede the

formation of shear structures. Whether this is the case for the fluorite-related oxides cannot definitely be decided from the present work. However, the appearance of single spots within the streaks observed in the

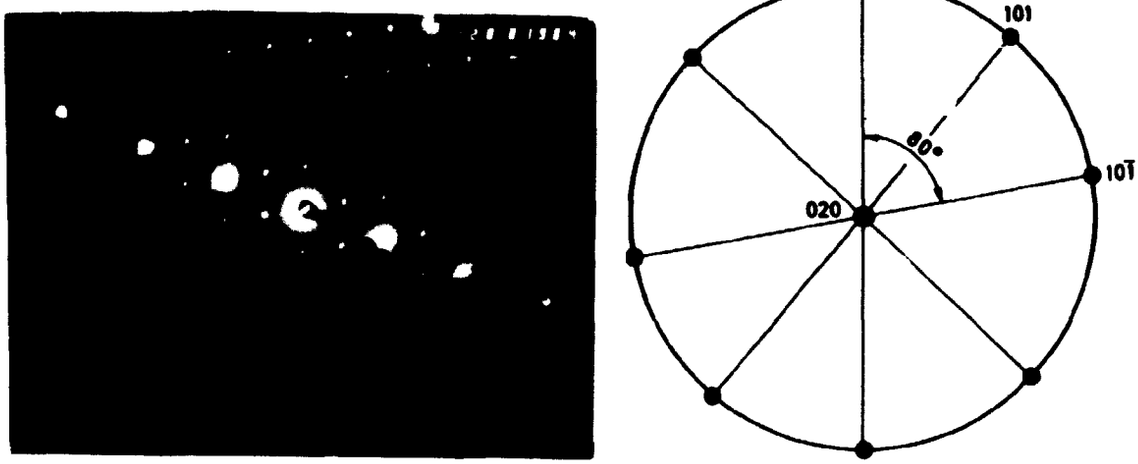

Fig. 24. Diffraction pattern of monoclinic superstructure ($P2_1/n$, C_{2h}^5) with $a = 6.781$, $b = 11.893$, $c = 15.823$ and $\beta = 125.04^\circ$. Indices shown on the stereographic projection. This structure was obtained by beam heating of the particle.

diffraction pattern for the sheared structure shown in fig. 21, showing that a new regular structure is being formed, seems to indicate that crystallographic shearing is more likely to take place for the fluorite-related oxides before a superstructure is formed.

4.3. Observations Made on Particles Heat-Treated in Vacuum

After the heat treatment in vacuum most of the diffraction patterns showed that the particles had broken up into polycrystalline, often textured aggregates, and it was very difficult to find patterns worth considering in greater detail. In a few cases, however, the (110) pattern shown in fig. 25 was obtained - similar patterns were also observed in the beam-heated particles.

From the figure it is clear that the extra spots do not lie in one specific direction, so the pattern does not originate from a structure formed by a crystallographic shearing mechanism. Assuming that twinning across the $\{\bar{1}12\}$ planes has taken place, the extra spots can be accounted for as shown in fig. 26, and it seems as if twinning is also possible in this oxide system.

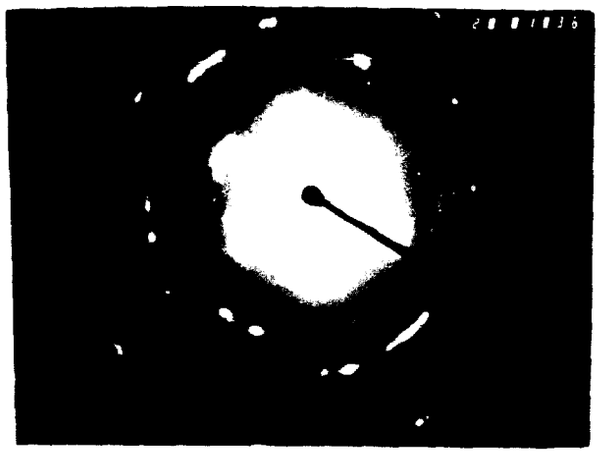

Fig. 25. (110) diffraction pattern for particle heat-treated in vacuum at 1440°C for 125 h. The pattern shows extensive twinning (compare to fig. 26).

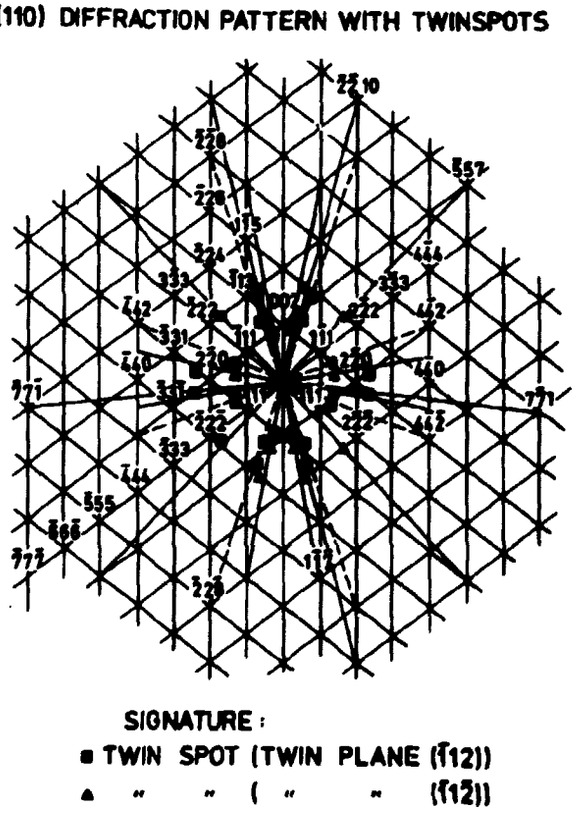

Fig. 26. Calculated (110) diffraction pattern for twinning on (1̄12) and (11̄2) respectively according to Hirsch (59). Near the centre spot matrix and twin spots form a hexagon, which is also observed in fig. 25. Double diffraction has not been considered in these calculations.

5. CONCLUSIONS

Summarizing the results obtained in the present work, the following conclusions can be drawn regarding the thermodynamic properties, phase relationships and structures of the CeO_{2-x}, PuO_{2-x} and $(U, Pu)O_{2-x}$ systems:

1) A detailed analysis of the thermodynamic data obtained by thermogravimetric equilibration measurements in atmospheres of controlled oxygen pressures (CO_2/CO mixtures) showed that the substoichiometric phase ranges for these oxides, which were previously described as grossly non-stoichiometric single phases, can be divided into several subregions. Thermodynamically, each of the subregions can be described by a characteristic value of the figure n, which according to defect theories describes the type of defect predominantly formed in the non-stoichiometric oxides. The defect theories are, however, based on assumptions which seem not to be fulfilled in practice - randomly distributed and non-interacting defects - and no firm conclusions regarding the actual defects present in the different subregions could be drawn from the present results.

2) Using the phase rule criteria for a binary oxide system in equilibrium with a gas phase, the nature of the subregions was inferred. For the three oxide systems investigated, this analysis showed that the subregions with $n \leq 6$ found in the range O/M: 200-1.875 consist of apparent non-stoichiometric single phases, whereas the $n > 6$ regions found at greater deviations from stoichiometry can be considered to consist of a sequence of discrete ordered phases separated by two phase regions. Besides these subregions, this analysis showed that discrete phases and two-phase regions not observed in previous studies are apparently formed for the PuO_{2-x} system in the composition range O/M ~ 1.995-1.950. A subregion consisting of two or more discrete phases was also observed for the $(U, Pu)O_{2-x}$ system near the stoichiometric composition. Neither have these phases been reported previously, although their existence can be inferred if the single data points of some of the previously published $\Delta\overline{G}_{O_2}$ versus composition curves are considered.

3) Supporting evidence for the existence of the observed subregions is also obtained from $\Delta\overline{G}_{O_2}$ versus T plots, which for constant composition give a straight line for each subregion. Furthermore, the relative partial enthalpies, $\Delta\overline{H}_{O_2}$, calculated from the slopes of these

vacuum at 1440°C for 125 h. The electron diffraction patterns obtained, as well as dark and bright field images, showed that a lamellae structure was obtained in some of the beam heated particles. A model involving crystallographic shearing along the $\{1\bar{2}1\}$ planes is proposed to explain this observation. In other particles the formation was observed of a monoclinic superstructure that closely corresponds to the superstructure found by the high temperature X-ray analysis. Electron microscopy examination of particles heat treated in vacuum showed that twinning across the $\{\bar{1}12\}$ planes can apparently also take place in these oxides.

The results obtained in the present work show that high resolution electron microscopy studies are essential for a complete understanding of this complex oxide system, and further studies with this technique appear to be especially fertile for future research.

11) D.J.M. Bevan and J. Kordis, J. Inorg. Nucl. Chem., 26 (1964) 1509-1523.

12) B.G. Hyde and L. Eyring, Phase Equilibrium and Phase Reactions in TbO_x-O_2 and Related System. In: Proceedings of the 4th Conference on Rare Earth Research April 22-25, 1964. Edited by L. Eyring (Gordon and Breach, New York, 1965) 623-664.

13) F.A. Kuznetsov, V.I. Belyi and T.N. Rezukhina, Proc. Acad. Sci. SSSR. Sec. Phys. Chem. 139 (1961) 642-645.

14) G. Brauer, K.A. Gingerich and U. Holtzschmidt, J. Inorg. Nucl. Chem. 16 (1960) 77-86.

15) D.J.M. Bevan, J. Inorg. Nucl. Chem. 1 (1955) 49-59.

16) G. Brauer and K.A. Gingerich, J. Inorg. Nucl. Chem. 16 (1960) 87-99.

17) B. Iwasaki and T. Katsura, Bull. Chem. Soc. Japan 44 (1971) 1297-1301.

18) J. Campserveux and P. Gerdanian, J. Chem. Thermodynamics 6 (1974) 795-800.

19) E.H. Greener, J.M. Wimmer, and W.M. Hirthe, Electrical Conductivity of Near-Stoichiometric a-CeO_2. In: Proceedings of the 3rd Conference on Rare Earth Research 1963. Edited by K.S. Vorres (Gordon and Breach, New York, 1964) 539-554.

20) C.J. Kevane, Phys. Rev. A133 (1964) A1431-A1436.

21) R.N. Blumenthal and J.E. Laubach, The Defect Structure of Non-Stoichiometric CeO_{2-x}. In: Anisotropy in Single-Crystal Refractory Compounds. Proceedings, held in Dayton, Ohio, 13-15 January 1967. Edited by F.W. Vahldiek and S.A. Mersol. Vol. 2 (Plenum Press, New York, 1968) 137-150.

22) R.N. Blumenthal, P.W. Lee, and R.J. Panlener, J. Electrochem. Soc. 118 (1971) 123-129.

23) P. Kofstad and A.Z. Hed, J. Amer. Ceram. Soc. 50 (1967) 681-682.

24) B.C.H. Steele and J.M. Floyd, Proc. Brit. Ceram. Soc. 19 (1971) 55-76.

25) R.J. Panlener and R.N. Blumenthal, Thermodynamic Study of Non-Stoichiometric Cerium Dioxide. COO-1441-18.

26) L.M. Atlas, J. Phys. Chem. Solids 29 (1968) 91-100.

27) F. A. Kröger, The Chemistry of Imperfect Crystals (North-Holland, Amsterdam, 1964) 1039 pp.

28) C. E. Holley, Jr., E. J. Huber, Jr., and F. B. Baker, Enthalpies, Entropies, and Gibbs Energies of Formation of the Rare Earth Oxides. In: Progress in the Science and Technology of the Rare Earth Research. Ed. by L. Eyring (Pergamon, Oxford, 1968) Vol. 3, 343-433.

29) D. Balesdent and L. Schuffenecker, C. R. Acad. Sci. Ser. C 272 (1971) 1703-1706.

30) L. A. Bursill and B. G. Hyde, Progr. Solid State Chem. 7 (1972) 177-253.

31) P. J. Hampson, Thermodynamic Properties of the Cerium-Oxygen System (General Electricity Research Laboratories) Laboratory Report RD/L/R 1843 (1973) 15 pp. + Appendix.

32) L. Manes, B. Manes-Pozzi, A Unified Model for Defects in Sub-Stoichiometric Plutonium Dioxide and Uranium-Plutonium Mixed Oxide. To be publiched in: Proceedings of 5th International Conference on Plutonium and other Actinides, September 1975 in Baden-Baden, Germany.

33) H. Blank, J. Nucl. Mat. 51 (1974) 269-270.

34) B. G. Hyde, D. J. M. Bevan, and L. Eyring, A Structural Model of the Rare Earth Oxides. In: I. Electron Diffraction. II. The Nature of Defects in Crystals. Abstracts of Papers presented at an International Conference, Melbourne, 16-21 August, 1965 (Pergamon Press, Oxford, 1966) II C-4.

35) M. R. Thornber, D. J. M. Bevan and J. Graham, Acta Cryst. B 24 (1968) 1183-1190.

36) A. Muan, The Use of Phase Diagrams in Metal, Refractory, Ceramic and Cement Technology. In: Phase Diagrams. Materials Science and Technology. Ed. by A. M. Alper (Academic Press, New York, 1970) Vol. 2.

37) R. R. Merritt and B. G. Hyde, Phil. Trans. Roy. Soc. London A 274 (1973) 627-661.

38) L. S. Darken and R. W. Gurry, Physical Chemistry of Metals (McGraw-Hill, New York, 1953) 535 pp.

39) A. Brown, X-Ray Powder Diffraction with Guinier-Hägg Focusing Cameras. AE-409 (1970) 51 pp.

40) A. Brown and A. Chitty, J. Nucl. Energy, Part B: Reactor Technology 1 (1960) 145-152.

41) M. Hoch and A. C. Momin, High Temp. - High Pressures 1 (1969) 401-407.

42) J. O. Sawyer, B. G. Hyde and L. Eyring, Bull. Soc. Chim. France 4 (1965) 1190-1199.

43) M. Z. Lowenstein, L. Kihlborg, K. H. Lau, J. M. Haschke, and L. Eyring, Growth and X-Ray Studies of Single Crystals of Higher Oxides of Praseodymium and Terbium. In: Solid State Chemistry. Proceedings of the 5th Materials Research Symposium, Gaithersburg, Md., 18-21 October 1971. Edited by Robert S. Roth and S. J. Schneider (USGPO, Washington, D. C., 1972) (National Bureau of Standards, Special Publication, 364) 343-351.

44) R. L. Martin, J. Chem. Soc. Dalton Trans. (1974) 1335-1350.

45) L. Eyring and B. Holmberg, Ordered Phases and Non-Stoichiometry in the Rare Earth Oxide System. In: Non-Stoichiometric Compounds (American Chemical Society, Washington, D. C., 1963) (Advances in Chemistry Series, 39) 46-57.

46) T. L. Markin, R. J. Bones, E. R. Gardner, Thermodynamic Data for Plutonium Oxides. AERE-R 4724 (1964) 17 pp.

47) L. M. Atlas and G. J. Schleeman, Defect Equilibria of PuO_{2-x}, 1100 to 1600°C. In: Thermodynamics. Proceedings, held in Wien, 22-27 July 1965. Vol. 2 (IAEA, Wien, 1966) 407-421.

48) L. M. Atlas and G. J. Schlehman, Defect Equilibria of Non-Stoichiometric Plutonium Dioxide 1045 to 1505°. In: Plutonium 1965. Proceedings, held in London, 22-26 November 1965. Edited by A. E. Kay and M. B. Waldron (Chapman and Hall, London, 1967) 838-844.

49) T. L. Markin and E. J. McIver, Thermodynamic and Phase Studies for Plutonium and Uranium-Plutonium Oxides with Application to Compatibility Calculations. In: Plutonium 1965. Proceedings, held in London, 22-26 November 1965. Edited by A. E. Kay and M. B. Waldron (Chapman and Hall, London) 845-957.

50) R. E. Woodley, J. Amer. Ceram. Soc. 56 (1973) 116-119.

51) N. A. Javed, J. Nucl. Mater. 43 (1972) 219-224.

52) The Plutonium-Oxygen and Uranium-Plutonium-Oxygen Systems: A Thermochemical Assessment. IAEA Technical Report Series No. 79 (1967) 86 pp.

53) P. Chereau, G. Dean, and P. Gerdanian, C.R. Hebd. Séances Acad. Sci. 272 (1971) 512-515.

54) T.L. Markin, R.S. Street, and E.C. Crouch, J. Inorg. Nucl. Chem. 32 (1970) 59-75.

55) LeRoy Eyring and Leung-Tak Tai, Annu. Rev. Phys. Chem. 24 (1973) 189-206.

56) R.J.D. Tilley, Crystallographic Shear in Inorganic Oxides. In: Solid State Chemistry. Edited by L.E.J. Roberts (Butterworths, London, 1972) (MTP International Review of Science. Inorganic Chemistry. Series One, 10) 279-313.

57) P. Kunzmann and LeRoy Eyring, J. Solid State Chem. 14 (1975) 229-237.

58) Metallurgy Department Progress Resport for the Period 1 Jan. - 31 Dec. 1974. Risø Report No. 327 (1975) 55 pp.

59) P.B. Hirsch et al., Electron Microscopy of Thin Crystals (Butterworths, London, 1965) 549 pp.

60) B.G. Hyde, Acta Cryst. A27 (1971) 617-621.

61) P. Gado, Acta Phys. Acad. Sci. Hung. 18 (1965) 111-117.

62a) J.S. Anderson and B.G. Hyde, Bull. Soc. Chim. France No. 4 (1965) 1215-1216.

62b) J.S. Anderson and B.G. Hyde, J. Phys. Chem. Solids 28 (1967) 1393-1408.

63) S. Andersson and A.D. Wadsley, Nature 211 (1966) 581-583.

64) J. Van Landuyt and S. Amelinckx, J. Solid State Chem. 6 (1973) 222-229.

APPENDIX

Construction and Testing of a Solid Electrolyte ZrO_2(CaO) Cell for Measurements of Partial Pressure of Oxygen in Furnace Atmospheres

In thermodynamic studies of oxides it is very important that the oxygen pressures of the atmospheres used can be determined accurately and for the studies described in this thesis a solid electrolyte ZrO_2(CaO) cell was constructed. The theory and principle of this cell, as well as its calibration, are described in this appendix.

1. THEORY

The most commonly used electrolyte for oxygen concentration cells is zirconia stabilized with calcia. Pure ZrO_2 crystallizes in a monoclinic ($T < 1200^{\circ}C$), tetragonal ($1200 < T < 2200^{\circ}C$) and cubic structure ($T > 2200^{\circ}C$) (1), but by addition of CaO from 12.5 to 22.5 mole % the cubic form can be stabilized to low temperatures (2). The non-stabilized structures show both ionic (3) and electronic conductivity (4, 5), whereas the stabilized cubic ZrO_2-CaO solid solutions show predominantly ionic conductivity within certain oxygen pressure ranges (6, 7), which makes these oxides especially suitable for oxygen concentration cells. By X-ray intensity measurements it has been shown (8) that, when added to ZrO_2, the divalent Ca-ions replace the tetravalent Zr-ions preferably on the (000) + fcc sites. Furthermore a corresponding number of oxygen vacancies in the anion lattice is formed to compensate for the charge difference between the Ca- and the Zr-ions; it is believed that these oxygen vacancies are responsible for the extensive ionic conductivity in these oxides.

The emf for a reversible cell of the type

$$Pt/P'_{O_2} \mid ZrO_2(CaO) \mid P''_{O_2}/Pt \qquad (1)$$

is given by (9):

$$E = \frac{1}{4F} \int_{\mu'_{O_2}}^{\mu''_{O_2}} t_{ion}\, d\mu_{O_2} \qquad (2)$$

where F is the Faraday equivalent, μ'_{O_2} and μ''_{O_2} the chemical potentials of oxygen on the two sides of the solid electrolyte, and t_{ion} the ionic transport number. According to the definition of chemical potentials

$$\mu_{O_2} = \mu^{o}_{O_2} + RT \ln P_{O_2} \tag{3}$$

and for $t_{ion} = 1$ the following expression can be obtained for E from equation 2:

$$E = \frac{RT}{4F} \ln \frac{P''_{O_2}}{P'_{O_2}} \quad . \tag{4}$$

At constant temperature a linear relationship thus exists between E and log P''_{O_2}/P'_{O_2}, and if, for instance, P''_{O_2} is kept constant by a continuous supply of air to this side of the electrode, the partial pressure of oxygen on the other side can be found by measuring the emf of the cell.

Within a certain range of partial pressure of oxygen ($100 \gtrsim P_{O_2} \gtrsim 10^{-22.5}$ atm) the electrical conductivity of $ZrO_2(CaO)$ is entirely ionic (6, 7, 10) and eq. (4) applies directly. Outside these limits, however, the electronic conductivity of the electrolyte becomes important. As the mobility of electrons is much higher than that of ions (14), and thus their contribution to the total conductivity is large, eq. (4) no longer applies, since

$$t_{ion} = \frac{\delta_{ion}}{\delta_{ion} + \delta_{el}} \tag{5}$$

is no longer equal to one. For the oxygen pressures where conduction of electrons becomes important, the emf for the cell will be changed according to (12):

$$E = \frac{RT}{4F} \ln P''_{O_2}/P'_{O_2} - \int_{\mu'_{O_2}}^{\mu''_{O_2}} t_{el}\, d\mu_{O_2} \tag{6}$$

where t_{el} = electronic transport number.

This equation, which can be derived from eq. (2) assuming that $t_{ion} + t_{el} = 1$, shows that the linear relationship between E and log P''_{O_2}/P'_{O_2} can no longer be expected when electronic conduction takes place, but that a decrease in E with increasing electronic conduction will be observed.

Besides electronic conduction, diffusion of oxygen molecules through the electrolyte will also limit the maximum temperature for these cells. This has not been examined for ZrO_2 stabilized with CaO, but for ZrO_2-MgO solid solutions, Möbius and Hartung (13) showed that diffusion of oxygen through this material takes place from about 850°C and that it increases exponentially with temperature. How serious the oxygen diffusion will be in an actual experimental set-up depends upon the geometry and the gas velocities used. It is also questionable how representative the permeability determined by Möbius and Hartung will be both for other MgO-stabilized ZrO_2 materials and for ZrO_2-CaO. Apparently oxygen diffusion in these materials takes place as grain boundary diffusion and not through porosities, or as volume diffusion. The permeability thus depends upon the fabrication technique and the content of impurities, which factors both influence the grain size of the material. To avoid errors due to molecular diffusion of oxygen through the cells, the maximum temperature should be limited, however, to about 1100°C until these problems have been examined more thoroughly.

There also seems to exist a lower temperature below which cell measurements become unreliable. This has been explained by the formation of Pt-oxides on the Pt-electrodes (14), which destroys the equilibrium between the electrodes and the electrolyte. If Pt-oxides are formed, they disproportionate at about 500°C (19), and it seems advisable not to work at temperatures lower than 700-800°C to avoid this trouble. This is also in accordance with Tretyakov (10), who claims that the lower temperature limit for ZrO_2(CaO) cells is about 700°C.

2. DESCRIPTION AND CONSTRUCTION OF CELL

2.1. Materials and Method of Construction

The cell was constructed from a Degussit ZR23 tube closed at one end. It had the following dimensions:

Outside diameter:	12.5 mm
Wall thickness:	2.0 mm
Length:	300 mm

The CaO content was analyzed to be 13.8 mole %. X-ray analysis showed the tube material to be single-phase solid solution with a lattice parameter of 5.11344 Å.

Porous platinum electrodes were applied inside and outside at the closed end of the tube and on an outside track along the tube by painting with platinum paste and firing in air at about 1000°C for about 5 hours using a heating and cooling rate of 100°C/h to avoid cracking the tube. After the first firing the electrode at the closed end of the tube appeared to be bright and to have good adherence, but a few bubbles had been formed in the track. To obtain low electrical resistance over the external electrode, the track was therefore repainted and refired twice, after which a resistance of 9 Ω could be measured over this electrode.

2.2. Principle of the Cell

The principle of the cell is shown schematically in fig. 1A.

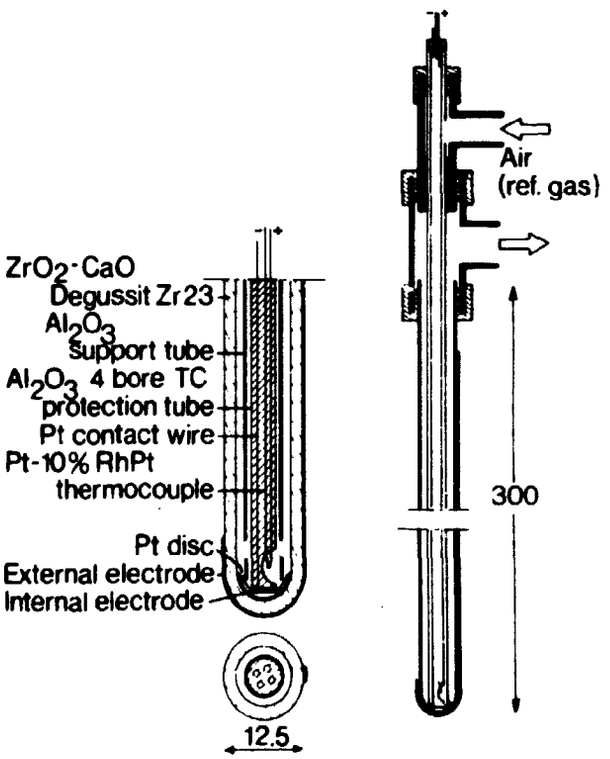

Fig. 1A. Principle of ZrO_2 (CaO) cell.

Contact to the internal platinum electrode was obtained with a platinum wire welded to a thin platinum disk that was pressed against the electrode with an aluminium support tube. A four-bore thermocouple protection tube placed inside this tube contained the contact wire as well as a Pt/Pt, Rh(10%) thermocouple. With flanges fastened gas-tight to the ZrO_2-tube and to the support tube, the system was arranged so that the reference gas could be supplied to the internal electrode through the support tube and then leave

the system through the space between the ZrO_2-tube and the support tube.

3. CALIBRATION OF THE CELL

3.1. Experimental

The cell was calibrated in CO_2/CO mixtures in the experimental set-up shown schematically in fig. 2A.

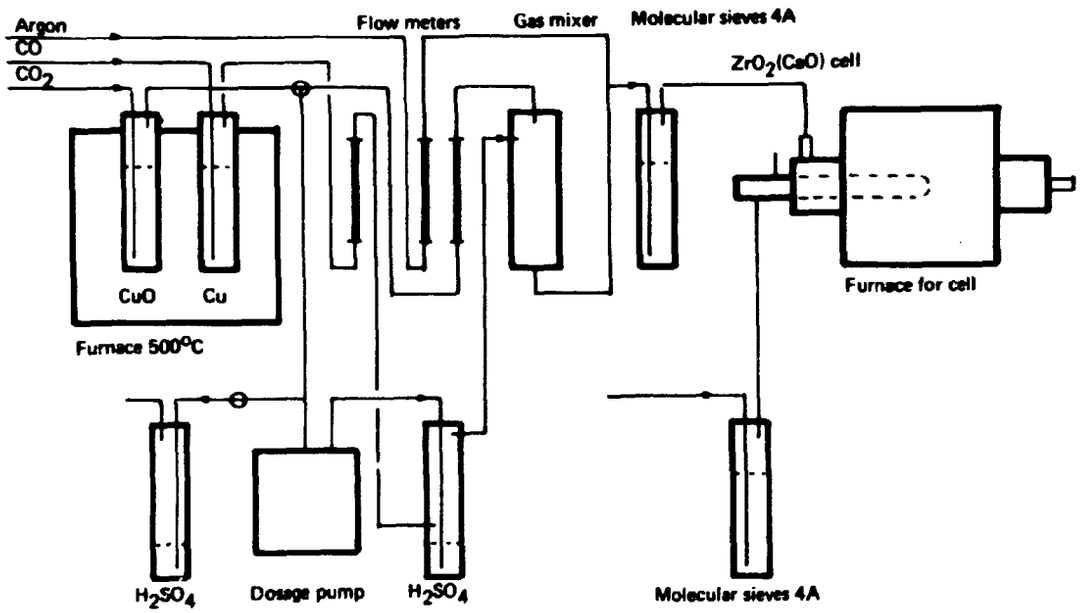

Fig. 2A. Experimental set-up for testing of the ZrO_2 (CaO) cell.

It consists of a gas system for purification and mixing of CO_2 and CO in the desired ratios and for the supply of Argon and air (reference gas) as well as a furnace in which the cell was placed in a Mullite tube. The cell was calibrated with CO_2/CO mixtures with the ratios 4/1; 2/3; 1/4; 1/10; 1/100 and 1/1000 at 800, 950 and 1100°C. The purity of the gases was checked by gas chromatographic analysis, which showed the following impurity contents:

CO: ≤0.03% O_2; ≤0.06% N_2; CO_2 not detected

CO_2: ≤0.5% air.

A difficulty often observed in experiments with gas mixtures is the segregation of the components due to thermal diffusion (15). In a experimental arrangement similar to our set-up Darken and Gurry (16) showed that for a 74% CO-26% CO_2 mixture the reduction in the CO content due to

thermal segregation could amount to 2.4% with a flow rate of 0.05 cm/sec, whereas this segregation was reduced to 0.2% at flow rates of 0.6 cm/sec or higher. Obviously flow rates lower than 0.6 cm/sec should be avoided and a gas flow of 20 l/h, corresponding to about 1 cm/sec in the cell furnace, was used in practically all the tests. In order to evaluate this effect a few tests were also carried out with a flow rate of 10 and 30 l/h.

The emf of the cell was measured with a digital voltmeter (Microvoltmeter M 441, Wagner Digital Elektronik, Berlin).

3.2. Theoretical emf Values

For the equilibrium between CO_2 and CO

$$CO_2 \rightleftharpoons CO + \tfrac{1}{2} O_2:$$

$$\log P_{O_2} = 2 \log K + 2 \log \left[\frac{CO_2}{CO}\right]_i \qquad (7)$$

where K = equilibrium constant and

$\left[\frac{CO_2}{CO}\right]_i$ = initial mixing ratio.

This equation applies as long as the CO_2/CO ratio is less than 100 (or vol% CO $>$ 1) (17), whereas for $[CO_2/CO]_i > 100$, the concentrations of O_2 and CO become comparable and a more accurate expression must be used.

In section 1 it was shown that

$$E = \frac{RT}{nF} \ln P''_{O_2}/P'_{O_2}, \qquad (8)$$

when electronic conduction is neglected. Using air as a reference gas ($P_{O_2} = 0.21$ atm), and substituting $\log P_{O_2}$ from eq. (7) into eq. (8), the following expression is obtained for the emf values:

$$E = -0.03369 \times T - 0.0496 \times T\left(2 \log K + 2 \log \left[\frac{CO_2}{CO}\right]_i\right) \qquad (9)$$

3.3. Results and Discussion

The emf values measured at 800, 950 and 1100°C are plotted in fig. 3A as a function of the oxygen pressures in the CO_2/CO mixtures used together with the theoretical emf values calculated from eq. (9) using the equilibrium constants given by Zeise (18).

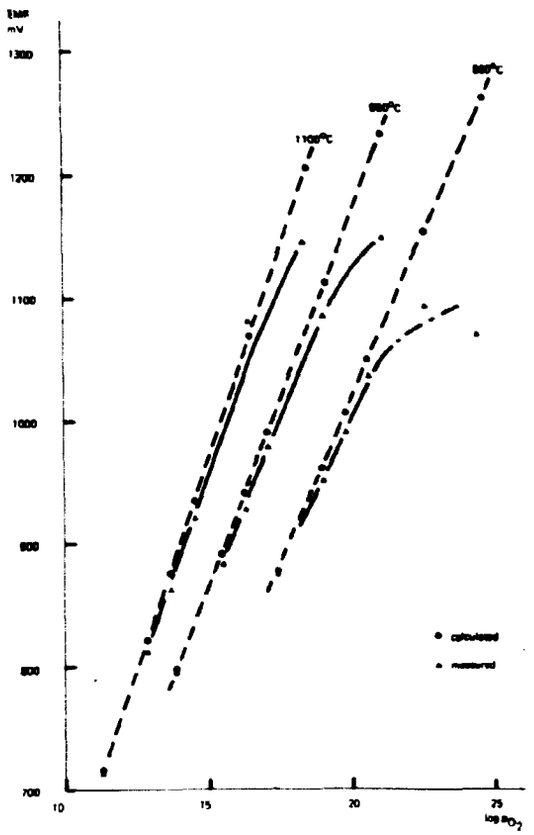

Fig. 3A. Measured emf values as a function of log P_{O_2} for CO_2/CO mixtures.

As shown in the figure the measured emf values vary linearly with log p_{O_2} above a certain oxygen pressure in accordance with the theoretical predictions. The values measured in this pressure range also closely correspond to the theoretical emf values, which were calculated under the assumption that $t_{ion} = 1$, and obviously the cell shows ionic conductivity in this range. At lower oxygen pressures, however, the measured emf values deviate significantly from the theoretical linear relationship indicating that electronic conduction becomes important.

For the three temperatures used in this work this effect is observed below the following oxygen pressures:

10^{-21} atm at 800°C

10^{-19} atm at 950°C

$10^{-17.5}$ atm at 1100°C

which give the lowest pressure limits at which it is recommended to use this cell. Compared to the critical pressures given in the literature for $ZrO_2(CaO)$, somewhat higher values are observed for this cell, probably because of a higher content of impurities in the commercial tube material used in this work.

In order to standardize the measurements a fixed temperature of 1000°C was chosen for the cell in the thermodynamic experiments. The calibration curve for this temperature, which was also determined with CO_2/CO mixtures, is shown in fig. 4A.

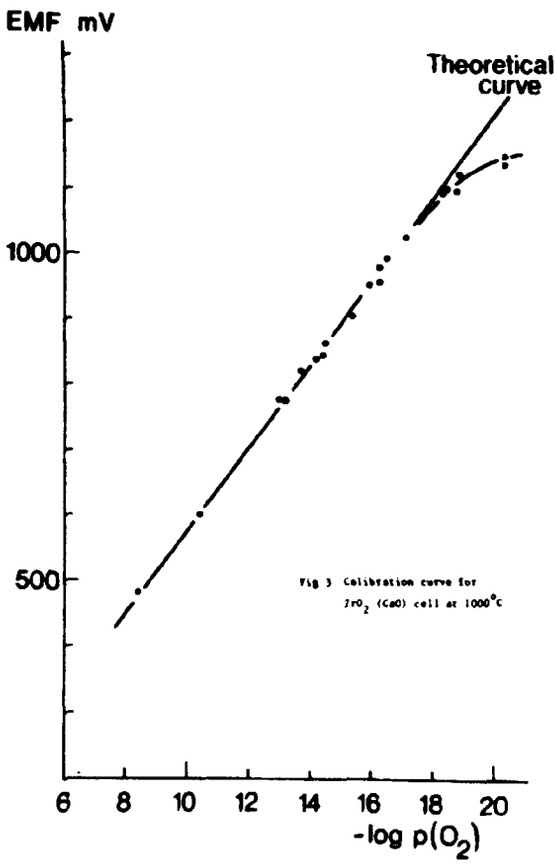

Fig. 4A. Calibration curve for the ZrO_2 (CaO) cell at 1000°C.

ACKNOWLEDGEMENT

The author wishes to thank H. Ringberg, AB Atomic Energy, Studsvik, Sweden, for his assistance with the construction and calibration of the cell.

REFERENCES FOR APPENDIX

1) G. M. Wolten, J. Am. Ceram. Soc. 46 (1963) 418-22.

2) H. A. Johansen and J. C. Cleary, J. Electrochem. Soc. 111 (1964) 100-103.

3) P. Kofstad and D. J. Rűzicka, J. Electrochem. Soc. 110 (1963) 181-84.

4) J. Rudolph, Z. Naturforsch. 14a (1959) 727-37.

5) R. W. Vest, N. M. Tallan, and W. C. Tripp, J. Am. Ceram. Soc. 47 (1964) 635-40.

6) K. Kiukkola and C. Wagner, J. Electrochem. Soc. 104 (1957) 379-87.

7) W. D. Kingery et al., J. Am. Ceram. Soc. 42 (1959) 393-398.

8) H. Schmalzried, Z. für Elektrochemie 66 (1962) 572-576.

9) C. Wagner, Z. Physik. Chem. Abt B 21 (1933) 25-41.

10) Ju. D. Tretyakov, J. Electrochem. Soc. 116 (1969) 331-334.

11) W. D. Kingery, Introduction to Ceramics (Wiley, New York, 1960) 781 pp.

12) B. C. H. Steele, High-Temperature Thermodynamic Measurements Involving Solid Electrolyte Systems. In: Proceedings of the Symposium on Electromotive Force Measurements in High-Temperature Systems, held in London, 1967 (Institution of Mining and Metallurgy, London, 1968) 3-28.

13) H. H. Möbius and R. Hartung, Silikattechnik 16 (1965) 276-281.

14) R. Hartung and H. H. Möbius, Z. Chem. 9 (1969) 197-198.

15) W. D. Kingery, Property Measurements at High Temperatures (Wiley, New York, 1959) 416 pp.

16) L. S. Darken and R. W. Gurry, J. Am. Chem. Soc. 67 (1945) 1398-1412.

17) K. Hagemark and M. Broli, J. Inorg. Nucl. Chem. 28 (1966) 2837-2850.

18) H. Zeise, Elektrochem. 43 (1937) 704-708.

19) A. Glasser, The Thermochemical Properties of the Oxides, Fluorides and Chlorides to 2500°K. ANL-5750 (1957) 70 pp.